

Towards a Comparison of the Folding of Prion Protein from Different Species

by

Sookpichaya Charrunchon

A thesis submitted in partial fulfillment of the requirements for the degree of

Master of Science

Department of Physics  
University of Alberta

© Sookpichaya Charrunchon, 2017

## **Abstract**

The formation of an abnormal form of proteins in cells can cause aggregation and neurodegenerative pathology, such as Alzheimer's, Parkinson's and prion diseases, which affects both humans and animals. Nowadays, the understanding of the mechanism of prion misfolding and propagation, including effective ways of treating prion diseases, is not clearly identified. This may result from the complexity of the biological ensembles.

Optical tweezers, one of the single-molecule force spectroscopy methods, can be used to better understand mechanisms of protein misfolding and dynamics by manipulating small beads attached to single protein molecules, resulting in the mechanical denaturation of protein structure. Previous work studying the mechanical denaturation of structure in hamster prion protein (PrP) by laser tweezers, for example, found that the folding pathways of the native protein were composed of two states of folding and unfolding (Yu et al., 2012; 2013).

Although the sequence of PrP is very highly conserved between species, there are a few differences in amino acid residues between PrP in different species. Furthermore, mouse PrP, a model system for studying prion diseases, has a lower susceptibility to the misfolding underlying prion diseases than hamster PrP. Thus, the differences in the protein sequences may lead to differences in the folding and misfolding which may relate to the different susceptibilities.

This work is the first single-molecule study of mouse PrP folding; the prion proteins from mice were attached to DNA handles using click chemistry and

were studied by optical tweezers in order to compare my results to those of the previous studies on hamster PrP. As a result of the successful attachments, the force-extension curves of mouse prion proteins had close similarities in unfolding behavior compared to those of hamsters. Furthermore, according to the data analysis of the curves, the contour lengths of the mouse prion proteins from the combination of rips were found to be closely matched to the expected length in the protein structure. However, it was challenging to avoid problems caused by attaching the DNA handles to the wrong cysteine residues in the protein.

For a more complete understanding of protein misfolding, future work involving the study of protein structure is required. Single-molecule studies of mouse prion proteins can also allow one to study the energy landscapes, specifically the folding pathways of proteins in different species. Information regarding protein structure may be useful for the development of specific therapeutic drugs. Future work on the molecular mechanisms of the prion proteins will not only provide a better understanding of prion diseases, but also other related neurodegenerative disease that share similar mechanisms of protein aggregation.

## Preface

This is the first single-molecule study of the folding of mouse prion protein, a model system for studying prion diseases, using optical tweezers. Manipulation of pairs of small beads connected by deoxyribonucleic acid (DNA) handles attached to mouse prion protein results in the mechanical denaturation of protein structure as revealed through the relationship between force and extension of the protein.

The expression and purification of prion protein were conducted by Craig Garen, a technician in the Woodside Lab. The initial protocols of the prion protein refolding, protein labelling with tetrazine, checking protein quality and secondary structural composition of the protein, and click chemistry attachment were provided by Dr. Derek Dee. I used and improved these protocols to prepare the protein samples with the assistance of Craig Garen and Dr. Derek Dee. The protocols for preparing transcyclooctene (TCO)-functionalised DNA primers using Reverse-Phase High Performance Liquid Chromatography (RP-HPLC) and using them to make DNA handles with the polymerase chain reaction (PCR) were provided by Dr. Derek Dee. I used these protocols to prepare handles with the assistance of Dr. Derek Dee, Meijing Wang, Mike Xia and Dr. Uttam Anand.

The measurements were done on laser tweezers at the National Institute for Nanotechnology maintained by Dushanth Seevaratnam, Dr. Supratik Sen Mojumdar, and Dr. Krishna Neupane. I used protocols for functionalising beads and measurement preparation was provided by Dr. Supratik Sen Mojumdar. Data collection and analysis were done by myself.

***“Everything in Life is Vibration” – Albert Einstein***

*In memory of*

*His Majesty King Chulalongkorn (1853 – 1910)*

*His Majesty King Bhumibol Adulyadej (1927 – 2016)*

## Acknowledgement

First of all, my deepest gratitude goes to the origin of the formation of elements for this interesting research and the opportunity to know the wonderful supervisor, Dr. Michael Woodside, who has tried to shed light on a better understanding of nature from a small detail by using single-molecule approach. He has introduced me to the fascinating world of prion protein, provided excellent guidance and also helped me develop a broader perspective on research.

I would like to express my sincere gratitude to the members of the supervisory committee, Dr. Frank Hegmann and Dr. Lindsay LeBlanc, and Associate Chair (Graduate Studies), Dr. Richard Marchand, for giving their valuable time to offer me insightful comments and directions through my program.

I would also like to extend my heartfelt appreciation to the members of the Woodside Lab, my collaborators, research technicians, and fellow graduate students: Craig Garen, the awesome technician in Woodside's Biochemistry laboratory, for his kindness and being ready to help, Dr. Derek Dee, a former postdoc, for teaching me Biochemistry method from making buffer to protein labelling, DNA primer purification and click chemistry, Meijing Wang for teaching me how to make DNA handles, run agarose gel and how to use UV-Visible spectroscopy, Joseph Jargstorf and Nichole Winczure for teaching me from basic Biochemistry knowledge to making SDS-PAGE gel, Mike Xia for teaching me to use CD Spectrometer and HPLC, Angela Briley for her willingness to help regarding Biochemistry stuff, Dr. Supratik Sen Mojumbar for teaching me from bead preparation to optical tweezers including data analysis and his kindness for being ready to help, Dr. Krishna Neupane for his willingness to help when I confronted with optical tweezers problem including data analysis, Dr. Dustin Ritchie for his wonderful brilliant knowledge and valuable guidance, Dr. Uttam Anand for his kindness, being ready to help and teach me from basic Biochemistry stuff to data analysis, Negar Rezajoei for teaching me from NanoDrop to data analysis, Dr. Rafayel Petrosyan for his interesting critical thinking and willingness to help others, Dr. Chunhua Dong for her kindness and being ready to help in

Biochemistry laboratory, Dr. Lindsay Shearer for her assistant and willingness to help from Biochemistry knowledge to English writing, Noel Hoffer, Dushanth Seevaratnam, Russell Kirchner and Matthew Halma for solving issues relating to optical tweezers, Tonia Cappellano, Zack Scholl, and all other current and former members of Woodside's group for making the laboratory a friendly environment.

Furthermore, my deepest appreciation is extended to the 20th Supreme Patriarch of Thailand, Somdet Amborn Ambaro, and my meditation master teacher, Phra Dhammongkolyarn, Luangphor Viriyang Sirintharo, for the precious knowledge to expand my consciousness and self-awareness.

I would also like to thank my parents who were the first wonderful teachers, my guidance and my inspiration, Mr. Suwapol and Ms. Assada Charrunchon, my first academic and research supervisor in Thailand since I was an undergraduate student, Dr. Nattaporn Chattham, my grandmom, Ms. Nob Kaewtathip, and my beloved brother, Mr. Phakchayot Charrunchon for their love, support and faith in me throughout my life. My heartfelt gratitude conveys to my close friends for always standing by my side including their love, precious friendship, wonderful encouragement, kindness and support: Mr. Phanuphong Jansorn, Mr. Polporn Apiwattanasawee, Mr. Rapeepat Hadkhanthung, Mr. Suphakorn Aunburom, Ms. Thanawan Poonsap, Ms. Thunyaporn Panyapan, Ms. Vararath Samerphop, and Mr. Worawut Bunnil. A special word of thanks also goes to all Thai people and international friends in Edmonton for the warmly welcome, especially to Ms. Alexandra Rodriguez, Mr. Dave Soltis - Ms. Katsuda Hemmarak, Mr. Jittichai Singhasiri - Ms. Vijittra Wattanasiri, Mr. Majid Nikouee, Ms. Maytave Boyd, Ms. Melissa Davis, Ms. Pittayapron Orathai, Mx. Sai Vemula, Mr. Sattar Soltani, Ms. Sherene Marie Gittens, Ms. Sumitra Chaiwong, Ms. Tareka Trakulsa and Ms. Teresa Kumblathan for their heart-warming kindness during my thesis writing.

Finally, I would like to thank and dedicate this thesis to the University of Alberta and National Institute for Nanotechnology (NINT) for providing me the real opportunity to broaden my perspective and conduct research with high profile professors, graduate students and international researchers.

## Table of Contents

1	Introduction .....	1
1.1	Protein Folding .....	1
1.2	Protein Misfolding .....	6
1.3	Prion Diseases .....	13
1.4	Outline of the Rest of Thesis .....	20
2	Single-Molecule Force Spectroscopy Studies .....	21
2.1	Optical Tweezers .....	21
2.2	Data Analysis .....	27
3	Sample Preparation .....	30
3.1	Prion Protein Expression and Purification.....	30
3.1.1	The expression of prion protein .....	30
3.1.2	The purification of prion protein.....	31
3.1.3	The refolding of prion protein.....	32
3.1.4	Circular dichroism spectra of prion protein .....	35
3.2	Protein Labelling.....	38
3.2.1	Prion protein labelling with tetrazine.....	38
3.2.2	Problem with the internal cysteine of prion protein.....	41
3.3	DNA Handles.....	47
3.3.1	Preparation of DNA primers .....	47
3.3.2	Preparation of DNA handles.....	50
3.3.3	Attachment of prion protein and DNA handles .....	53
3.4	Preparation for The Pulling Measurement.....	56

4	Results.....	57
4.1	Force-Extension Curves of the Handle-Handle Attachment .....	57
4.2	Force-Extension Curves of the Mouse Prion Protein (MoPrP) .....	61
4.3	Force-Extension Curves of Prion Proteins from Different Species .....	67
5	Future Works .....	71
	Bibliography .....	75

## List of Tables

Table 1.1 Examples of human diseases associated with protein aggregation.....	7
Table 1.2 List of the different mechanisms resulting from misfolded protein conformers and the misfolding diseases in the perspective of gain and loss of function. ....	9
Table 1.3 Experimental approaches to investigate the study of protein folding and aggregation.....	11
Table 1.4 Comparison of prion protein diseases.....	15
Table 1.5 Species susceptibility to Chronic wasting disease (CWD) infection.....	17
Table 2.1 The methods for the mechanical manipulation of single molecules by stretching of the molecules in elongation flow .....	22
Table 3.1 PCR Mixture for DNA handle .....	51
Table 3.2 The PCR program set-up .....	52

## List of Figures

Figure 1.1 Illustration of the structure of an amino acid.....	1
Figure 1.2 Schematic of the peptide bond formation.....	2
Figure 1.3 Ramachandran diagrams and the secondary protein structures.....	3
Figure 1.4 An idealized funnel landscape.....	4
Figure 1.5 Pathway of aggregation.....	6
Figure 1.6 Schematic energy landscape for protein folding, misfolding and aggregation.....	10
Figure 1.7 The structures of the cellular prion protein (PrP <sup>c</sup> ).....	14
Figure 1.8 Representative sequence alignment of mammalian prion proteins.....	18
Figure 2.1 Optical tweezers diagram.....	25
Figure 2.2 Single-beam optical tweezers apparatus.....	26
Figure 2.3 Schematic of the dual-beam optical tweezers for the prion protein stretching experiment.....	26
Figure 2.4 Force-extension curve of the protein-DNA handle attachment and the DNA handles.....	27
Figure 2.5 Ten unfolding force-extension curves of protein (red traces) fitting to the WLC model.....	29
Figure 3.1 Representative elution profile of the mouse prion protein (MoPrP) purification on the column diagram.....	32
Figure 3.2 Analysis of mouse prion protein fractions in SDS-PAGE.....	34
Figure 3.3 CD Spectra of poly-L-lysine.....	35

Figure 3.4 Comparison between the CD Spectrum of mouse prion protein that successfully attached to the DNA and unsuccessfully attached to the handle.....	36
Figure 3.5 Representative CD Spectra of mouse prion protein after the refolding procedure.....	37
Figure 3.6 The ultraviolet absorption of mouse prion protein (MoPrP) and mouse prion protein labelled with tetrazine (MoPrp+Tz).....	40
Figure 3.7 SDS-PAGE Analysis of mouse prion protein and Cy5-TCO.....	41
Figure 3.8 Sequence of the wild type mouse prion protein .....	41
Figure 3.9 SDS-PAGE Analysis of mouse prion protein labelled with tetrazine using TCEP and Cy5-TCO from Derek Dee .....	43
Figure 3.10 SDS-PAGE Analysis of mouse prion protein labelled with tetrazine using MEA and Cy5-TCO from Derek Dee .....	44
Figure 3.11 Representative CD Spectrum of mouse prion protein and mouse prion protein labelled with tetrazine.....	46
Figure 3.12 The ultraviolet absorption of the collected 802 bp (base pairs) TCO primer .....	48
Figure 3.13 The ultraviolet absorption of the collected 2110 bp TCO primer .....	49
Figure 3.14 HPLC profile of the 250 $\mu$ M of Cy5-Tz for the quality control.....	49
Figure 3.15 UV absorbance spectra of the TCO primer and the TCO primer + Cy5-Tetrazine (Cy5 Tz).....	50
Figure 3.16 Representative agarose gel electrophoresis of the DNA handle .....	53
Figure 3.17 Reaction scheme for conjugation of tetrazine-modified protein with TCO modified handle .....	53
Figure 3.18 Representative agarose gel electrophoresis of the DNA handle-DNA handle attachment .....	54
Figure 3.19 Representative agarose gel electrophoresis of the protein-DNA handle attachment compared to the DNA handle-DNA handle attachment .....	55

Figure 3.20 Representative agarose gel electrophoresis of the unsuccessful protein-DNA handle attachment compared to the DNA handle-DNA handle attachment .....	55
Figure 3.21 Schematic of the sample for the pulling measurement.....	56
Figure 4.1 Representative force-extension curve measurement of the 802 bp TCO and 1265 bp TCO handle attachment.....	58
Figure 4.2 Representative force-extension curve measurement of the 802 bp TCO and 2110 bp TCO handle attachment.....	59
Figure 4.3 Representative force-extension curve measurement of the 802 bp Tz and 2110 bp TCO handle attachment.....	59
Figure 4.4 Analysis of force spectroscopy measurement consisting of WLC fit to DNA handle (pink) and determine contour length of protein (green) .....	61
Figure 4.5 Optical tweezers apparatus for the mouse prion protein stretching experiment.....	62
Figure 4.6 Representative force-extension curve measurement of the mouse prion protein attached to the 802 bp TCO and 2110 bp TCO handle .....	63
Figure 4.7 Example of incorrectly formed tethers of the mouse prion protein attached to the 802 bp TCO and 2110 bp TCO handle.....	64
Figure 4.8 The possibility of the shorter length of mouse prion protein .....	66
Figure 4.9 Representative force-extension curve measurements of hamster prion protein from Hao Yu.....	68
Figure 4.10 Representative force-extension curve measurements of rabbit prion protein from Uttam Anand.....	68
Figure 4.11 The sequence of hamster, mouse and rabbit prion proteins .....	70

## List of Symbols, Nomenclatures, or Abbreviations

2Cys-MoPrP	mouse prion protein that was specially engineered to have the cystines the both ends
A	Alanine (amino acid residue)
A (state)	amyloid fibril
A <sub>260</sub>	absorbance at 260 nm
A <sub>280</sub>	absorbance at 280 nm
AFM	Atomic force microscopy
AFS	Acoustic Force Spectroscopy
ALS	Amyotrophic Lateral Sclerosis
amu	atomic mass unit
ANS	1-anilino-8- naphthalene sulfonic acid
APS	Ammonium persulfate
BFP	Biomembrane Force Probe
bp	base pairs
BSE	Bovine Spongiform Encephalopathy
C	Cystine (amino acid residue)
C $\alpha$	central carbon atom
CC	charged cluster
CD	circular dichroism
CFTR	Cystic fibrosis transmembrane conductance regulator
CJD	Creutzfeldt-Jacob's disease
CWD	Chronic Wasting disease
Cy5	Cyanine5
D	Aspartate (amino acid residue)
DMSO	Dimethyl Sulfoxide Hybri-Max <sup>TM</sup>
DNA	deoxyribonucleic acid
dNTP	Deoxynucleotide
dsDNA	double stranded DNA
EDTA	Ethylenediaminetetraacetic acid
ER	endoplasmic reticulum
EtBr	ethidium bromide

FEC	force-extension curve
FTD	Frontotemporal dementia
F(x)	applied force as a function of extension
G	Glycine (amino acid residue)
g	gram
Gb3	Glycosphingolipid globotriosylceramide
GdnHCl	guanidine hydrochloride
GPI	glycosyl phosphatidyl inositol
GSH	L-Glutathione reduced
GSSG	Glutathione oxidized
H	Histidine (amino acid residue)
HC	hydrophobic core
I	Isoleucine (amino acid residue)
IPTG	isopropyl $\beta$ -D-1-thiogalactopyranoside
K	Lysine (amino acid residue)
K	elastic modulus
KCl	potassium chloride
kDa	kilodalton
KH <sub>2</sub> PO <sub>4</sub>	monopotassium phosphate
l	litre
L	Leucine (amino acid residue)
L <sub>c</sub>	contour length
L <sub>p</sub>	persistence length of the chain
LB	Luria-Bertani
m	mili (unit prefix)
M	Methionine (amino acid residue)
M	Molar
MA	membrane anchor region
mal-PEG4-Tz	maleimide - polyethylene glycol 4 - tetrazine
MEA	cysteamine hydrochloride
MgCl <sub>2</sub>	magnesium chloride
MoPrP	mouse prion protein

MWCO	Molecular weight cut-off
n	nano (unit prefix)
N	Asparagine (amino acid residue)
N (state)	native state
NaCl	sodium chloride
Na <sub>2</sub> HPO <sub>4</sub>	disodium hydrogen phosphate
NaH <sub>2</sub> PO <sub>4</sub>	monosodium phosphate
NaOAC	sodium acetate
NHS	N-Hydroxysuccinimide
nm	nanometer
NMR	Nuclear Magnetic Resonance
O (state)	small oligomer
OD <sub>600</sub>	UV spectroscopy measured at a wavelength of 600 nm
oligos	oligonucleotides
p	pico (unit prefix)
P	Proline (amino acid residue)
PBS	Phosphate-buffered saline
PCR	polymerase chain reaction
PEG	polyethylene glycol
PK	proteinase K
PMSF	phenylmethane sulfonyl fluoride
PrP <sup>c</sup>	prion protein or a normal cellular prion protein
PrP <sup>sc</sup>	infectious prion protein
Q	Glutamine (amino acid residue)
R	Arginine (amino acid residue)
R	unique side-chain
R-plot	Ramachandran plot
RBC	Red blood cell
RP-HPLC	Reverse-Phase High Performance Liquid Chromatography
ref	relative centrifugal force
rpm	revolutions per minute
S	Serine (amino acid residue)

S-S	single disulfide
SC	Scrapie
SDS	sodium dodecyl sulphate
SDS-PAGE	sodium dodecyl sulphate-polyacrylamide gel electrophoresis
SMFS	single-molecule force spectroscopy
T	Threonine (amino acid residue)
TBE	tris-borate-ethylenediaminetetraacetic acid
TCEP	tris(2-carboxyethyl)phosphine
TCO	transcyclooctene
TEMED	Tetramethylethylenediamine
Titin	giant filamentous polypeptide
Tris	trisaminomethane
TSEs	transmissible spongiform encephalopathies
Tz	tetrazine
Tz-PEG	bis-tetrazine- polyethylene glycol
U (state)	unfolded or partially folded states
UV	ultraviolet
UV-Vis	Ultraviolet–visible spectroscopy
V	Valine (amino acid residue)
V	Volt
W	Tryptophan (amino acid residue)
Water	H <sub>2</sub> O
WLC	wormlike chain
WT-MoPrP	wild type mouse prion protein or normal mouse prion protein
x	extension
Y	Tyrosine (amino acid residue)
-COOH	carboxyl group
-NH <sub>2</sub>	amine group
α	alpha
β	beta
βME	beta-mercaptoethanol

$\mu$	micro (unit prefix)
$\phi$	phi angle
$\psi$	psi angle
$\omega$	omega angle

# 1. Introduction

## 1.1 Protein Folding

The four important chemical building blocks of life are proteins, nucleic acids, lipids and carbohydrates (Raven and Johnson, 2001). They perform different functions in cells. For example, the chemistries of the cell (cell signaling, metabolism and immune response) are performed by proteins, the genetic information is stored and transferred by nucleic acids, some parts of the cell membrane are formed by lipids, and some building materials in cells are provided by carbohydrates.

Although proteins can perform many important roles, there are only 20 types of amino acids resulting from a unique side-chain (R) attached to the central carbon atom ( $C_{\alpha}$ ) in each amino acid, as shown in figure 1.1. The differences between amino acids can be determined into 3 groups, namely, the non-polar, the polar and the charged amino acids. The simplest amino acid is glycine (G), consisting of only one hydrogen atom in the side-chain.

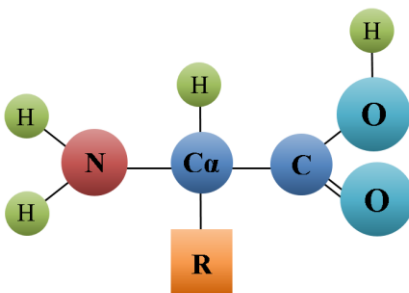


**Figure 1.1 Illustration of the structure of an amino acid.** The central carbon atom ( $C_{\alpha}$ ) contains a hydrogen atom, an amine group ( $-NH_2$ ), a carboxyl group ( $-COOH$ ) and a specific side-chain group (R) for each amino acid.

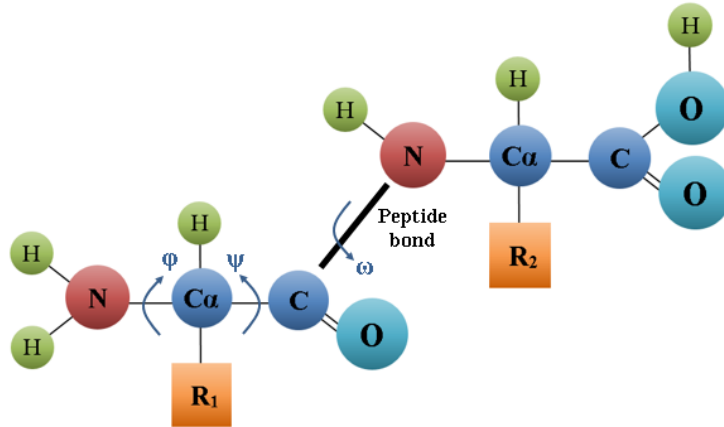


**Figure 1.2 Schematic of the peptide bond formation.** Two amino acids are linked together via peptide bond resulting in the polypeptide structure. On both sides of the central carbon atom ( $C\alpha$ ) consist of two rotation angles defined as  $\phi$  and  $\psi$ , as shown in the diagram.

Another interesting polar amino acid is cysteine (C), because it has the ability to form a strong disulfide bond to another cysteine residue, which can play an important role in protein structure or interactions between molecules. The linear sequence of amino acids in a protein molecule attached in that specific order via peptide bonds is called the primary structure.

There are three angles of rotation around the bonds in the main chain of protein or the protein backbone as shown in figure 1.2. The most two important angles to determine the structure of proteins are the dihedral angles consisting of the phi ( $\phi$ ) angle, the angle around N- $C\alpha$  bond, and the psi ( $\psi$ ) angle, the angle around  $C\alpha$ -C bond. The combinations of the different dihedral angles result in the different secondary structures of proteins, such as the alpha helix ( $\alpha$ -helix) and the beta sheet ( $\beta$ -sheet) structures shown in figure 1.3 (Ramachandran et al., 1963). There are two types of the  $\alpha$ -helix structures, left handed and right handed, located in the upper right quadrant and the lower left quadrant of the Ramachandran plot,

respectively. The broad region in the left quadrant with the average  $\phi$  and  $\psi$  angle of  $-120^\circ$  and  $120^\circ$  is the  $\beta$ -sheet structure, associated with the formation of amyloid fibrils which are a symptom in many neurodegenerative diseases. The packing of  $\alpha$ -helix and  $\beta$ -sheet elements connected by loops or turns results in the formation of a third level in the hierarchy of structure, tertiary structure (Anfinsen, 1973; Chothia, 1976).

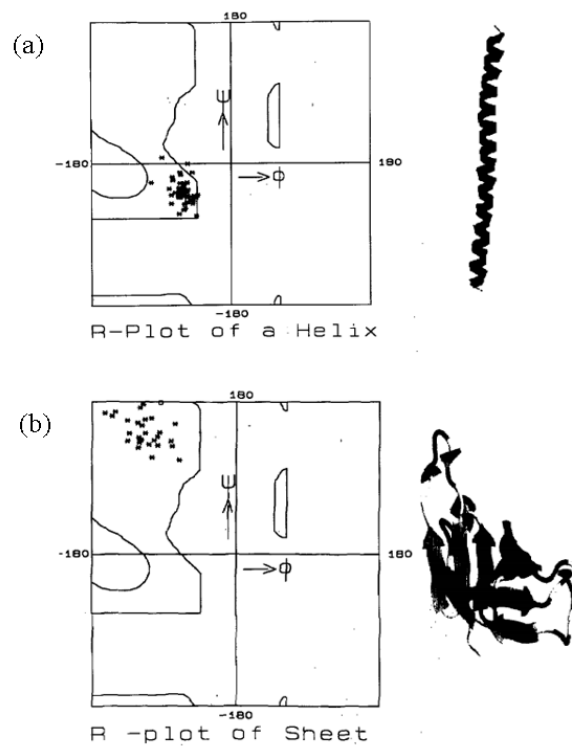


**Figure 1.3 Ramachandran diagrams and the secondary protein structures.** The common secondary structures of proteins are in three allowed regions in the Ramachandran plot (R-plot). (a) The clusters in the lower left quadrant represent the right handed  $\alpha$ -helix proteins, which the ribbon diagram of the segment is shown on the right. (b) The combinations of dihedral angles of the  $\beta$ -sheet structures are located in the upper left quadrant in the R-plot, and the corresponding diagram of the structure is on the right, reproduced from (Ramakrishnan, 2001).

Protein structures are held together by many interactions, such as hydrophobic interactions, electrostatic interactions, Van der Waals interactions and hydrogen bonds. In the early 1960s, Anfinsen and co-workers proposed that the native structures of small proteins are thermodynamically stable states which are not determined by the folding route but by the lowest free energy, in a manner depending on the amino acid sequence and the conditions of the solution (Anfinsen et al., 1961; Anfinsen, 1973; Dill et al., 2008). However, in the late 1960s, Levinthal made the argument that a random search for native structure would take too long; hence, there should be a specific folding pathway for proteins in order to be folded within the realistic timeframe of microseconds to seconds (Dill and Chan, 1997; Levinthal, 1969). The relationship between free energy and protein conformation is called energy landscape as shown in figure 1.4.

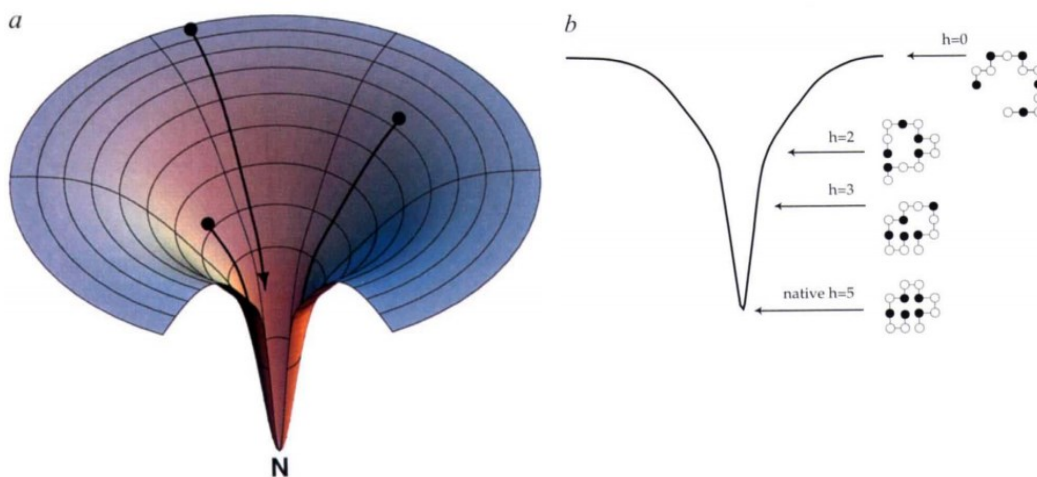


**Figure 1.4 An idealized funnel landscape.** The increase of the numbers of intrachain contacts results in the decrease of its internal free energy. There is only one conformation of its final native state that has the minimum of free energy. Note: The black and white beads represent hydrophobic monomers and hydrophilic monomers, respectively, and  $h$  is the number of hydrophobic contacts, reproduced from (Dill and Chan, 1997).

In order to be functional in cells, proteins should generally be in the correct structure or native state. If not, a “misfolded” protein may not function correctly and might interact improperly or form aggregates leading to diseases such as Alzheimer’s disease, Parkinson's disease, Amyotrophic Lateral Sclerosis (ALS), Lysozyme amyloidosis, Type II diabetes, and prion diseases (Chiti and Dopson, 2006; Ross and Poirier, 2004). Therefore, this work has been focused on the understanding of misfolding in the prion protein, whose misfolding causes the family of prion diseases.

## 1.2. Protein Misfolding and Diseases

There are mechanisms in nature to eliminate the misfolded proteins in cells. For example, proteasomes prevent the accumulation of toxic proteins by degrading them and chaperones assist proteins to fold into the correct structures (Ellis, 2006; Goldberg, 2003). However, fibrillar aggregates of protein with  $\beta$ -sheet structures, called amyloid fibrils, are stable and insoluble leading them to be highly resistant and rarely degradable (Eisele et al., 2015). Amyloid fibril formation by misfolded proteins can be adopted under various stress factors or the conditions that the native structure was destabilized resulting in numerous neurodegenerative diseases (Fändrich et al. 2001; Fink, 1998; Stathopoulos et al., 2004). These diseases can be categorized into three groups (neurodegenerative diseases, non-neuropathic systemic amyloidosis and non-neuropathic localized amyloidosis) corresponding to the different locations of protein aggregation such as the brain, single types of tissues and multiple tissues, respectively, as shown in table 1.1 (Knowles et al., 2014; Soto, 2001).

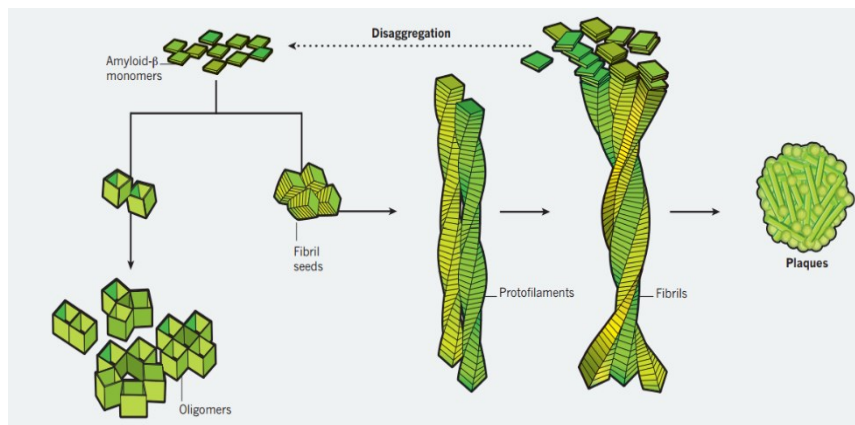


**Figure 1.5 Pathway of aggregation.** The amyloid- $\beta$  peptides can be assembled in order to form soluble oligomers or insoluble fibrils resulting in neurodegenerative diseases, reproduced from (Schnabel, 2011).

**Table 1.1 Examples of human diseases associated with protein aggregation,** adapted from (Chiti and Dopson, 2006; Knowles et al., 2014; Sacchettini and Kelly, 2002).

<b>Diseases</b>	<b>Aggregation proteins</b>	<b>Number of amino acids</b>
<b>Neurodegenerative diseases</b>		
Alzheimer's disease  (The most common form of dementia including memory loss and difficulty with thinking)	Amyloid- $\beta$ peptide	37–43
Frontotemporal dementia (FTD) with Parkinsonism  (Disorder of brain affected language skills, behavior and movement)	Tau	352–441
Huntington's disease  (Brain disorder resulted in emotional problems, uncontrolled movements and loss of thinking skills)	Huntington fragments	Variable
Parkinson's disease  (Disorder of nervous system affected the motor system involving with the movement)	$\alpha$ -synuclein	140
Spongiform encephalopathies  (Rare degenerative disorder affected brain and nervous system of humans and animals)	Prion protein or its fragments	230
<b>Non-neuropathic systemic amyloidosis</b>		
Fibrinogen amyloidosis  (A systemic amyloid disease resulting in abnormalities in kidney function)	Variants of fibrinogen	27–81

Haemodialysis-related amyloidosis  (Disabling disease resulted in progressive loss in kidney function)	$\beta$ 2 -microglobulin	99
Lysozyme amyloidosis  (Systemic non neuropathic amyloidosis disease leading to gastrointestinal symptom)	Lysozyme mutants	130
<b>Non-neuropathic localized amyloidosis</b>		
Injection-localized amyloidosis  (A rare condition occurred in diabetic patient who do not alter the insulin injection site)	Insulin	21 and 30
Pituitary prolactinoma  (The most common type of pituitary tumor resulted in irregular menstrual periods in women or vision loss (large tumor size))	Prolactin	199
Type II diabetes  (The most common form of diabetes leading to the high level of glucose in blood)	Amylin	37

However, according to the perspective of gain and loss of function, the neurodegenerative diseases from protein misfolding can be divided into two groups, such as a gain of toxic function and a loss of physiological function, as shown in table 1.2 (Soto, 2001; Winklhofer et al., 2008).

**Table 1.2 List of the different mechanisms resulting from misfolded protein conformers and the misfolding diseases in the perspective of gain and loss of function, adapted from (Soto, 2001; Winklhofer et al., 2008).**

<b>Gain of toxic function transformations</b>		<b>Loss of function transformations</b>	
<b>Mechanisms</b>	<b>Involved protein</b>	<b>Mechanisms</b>	<b>Involved protein</b>
Lysosomal degradation	$\alpha$ -synuclein, Prion protein	Impairment of synaptic dynamics	$\alpha$ -synuclein
Neurotoxic signaling	Prion protein	Increased vulnerability to stress	Prion Protein
Pore formation	$\alpha$ -synuclein	Loss of trophic support	Progranulin
Synaptic deficits	Amyloid- $\beta$ peptide, tau, Prion protein	Mitochondrial dysfunction	Parkin
<b>Diseases</b>	<b>Involved protein</b>	<b>Diseases</b>	<b>Involved protein</b>
Alzheimer's disease	Amyloid- $\beta$ peptide	Cystic fibrosis (Common fatal genetic disease in young Canadians affected the digestive system and lungs)	Cystic fibrosis transmembrane conductance regulator (CFTR) protein
Huntington's disease	Huntington fragments	Fabry's Disease (Inherited disorder resulted in episodes of pain, especially in hands and feet)	Glycosphingolipid globotriosylceramide (Gb3)

Parkinson's disease	$\alpha$ -synuclein	Sickle cell anemia  (Blood disorder leading to anemia or blocking blood flow resulted in pain and organ damage)	Hemoglobin
---------------------	---------------------	---	------------

In a stressed environment, proteins with rich  $\beta$ -sheet content can be aggregated resulting in the complicated and rugged free energy landscape, as shown in figure 1.6. The partially folded states of a protein can be either native or misfolded structures depending on their energies, energy barriers and the presence of folding assistant proteins, such as chaperones and proteasomes (Amm et al., 2014; Hartl et al., 2011).

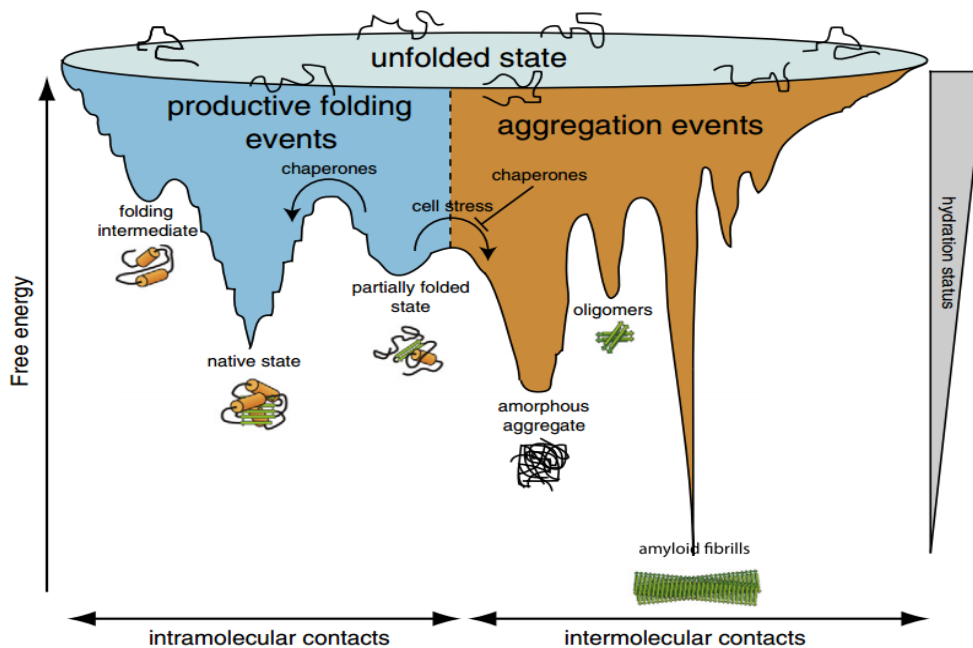


**Figure 1.6 Schematic energy landscape for protein folding, misfolding and aggregation.** Normal proteins tend to enter an energetically favourable folding path at the lowest free energy in productive folding events resulting in the native state. According to the stress environment, if proteins are not disrupted by chaperones, the proteins can be aggregated leading to the formation of toxic oligomers or amyloid fibrils as shown in the aggregation events, reproduced from (Amm et al., 2014).

In order to characterize the free energy landscape of the protein folding and aggregation, many experimental approaches have been developed to monitor proteins in terms of structural characterizations or mechanisms as shown in table 1.3 (Dobson, 2004; Jahn and Radford, 2005). In this study, the prion protein, which can misfold to cause neurodegenerative diseases, was studied by using the single molecule approach (optical tweezers).

**Table 1.3 Experimental approaches to investigate the study of protein folding and aggregation.** Note: U, N, O and A represent unfolded or partially folded states, native state, small oligomer and amyloid fibril, respectively, adapted from (Bartlett and Radford, 2009; Dobson, 2004; Jahn and Radford, 2005; Plaxco and Dobson, 1996)

Property	Technique	Measurement	Proteins
Chain Packing	Intrinsic tryptophan fluorescence	The intensity of orientation and environment of tryptophan	U,N,O,A
	ANS (1-anilino-8- naphthalene sulfonic acid) binding	Formation and disruption of hydrophobic patches and clefts to exposure of the aromatic surface area	U,N,O,A
Molecular dimensions	Fluorescence anisotropy	The mobility of tryptophan and overall molecular dimensions to determine shape and size of molecule	U,N,O,A
	Small angle X-ray scattering	The average radius of gyration to obtain three-dimensional structure information	N,O

Secondary structure and persistent hydrogen bond	Far-ultraviolet (UV) circular dichroism	Backbone conformation averaged over sequence and population for the interpretation of structure content	U,N,O,A
	Pulse labelling mass spectrometry	The formation of persistent hydrogen bonds for the qualification of the different hydrogen-exchange populations	U,N,O,A
	Pulse labelling Nuclear Magnetic Resonance (NMR)	Sequence specific formation to identify the hydrogen-exchange behavior of the stable amide and tryptophan hydrogen bonds	U,N
Tertiary contacts and native structure	Protein engineering	The energetic contributions of the side chains to determine the rate of folding and stability of a species of interest	U,N
	Real time NMR spectroscopy	Formation of specific side chain tertiary contacts for the analysis of denatured states and intermediates in slowly folding proteins	U,N
	Single molecule experiment (Atomic force microscopy (AFM), optical tweezers)	The relationship between force required to unfolded protein and extension	U,N

### 1.3. Prion Diseases

Prion Protein (PrP) is a protein present in vertebrates and mammals (Collinge, 2016; Prusiner, 1982). The structure of PrP in its cellular form consists of an amino-terminal signal peptide for guiding protein to the endoplasmic reticulum (ER), an unstructured N-terminal domain, and an alpha-helical C-terminal domain containing the attachment region to the cell membrane via the glycosyl phosphatidyl inositol (GPI) anchor, as shown in figure 1.7 (Aguzzi and Heikenwalder, 2006; Gossert et al., 2004).

The level of PrP expression is highest in nervous tissues, whereas the lower expression levels are found in the skin, blood and gastrointestinal tract (Davies et al., 2006). Many different functional roles have been proposed for PrP, such as copper binding, cellular iron uptake, cell adhesion, molecule recognition, junction-associated protein distribution and epithelial cell proliferation (Brown et al., 1997; Morel et al., 2008; Martins et al., 2001; Singh et al., 2009; Westergard et al., 2007). Furthermore, according to the localization of the prion protein on the cell membrane, PrP could have some potential roles associated with the cell signaling pathways, such as those in the migration of brain microvascular endothelial cells and the involvement of signal transduction in neurite outgrowth and neuronal survival (Chen et al., 2003; Watanabe et al., 2011).

However, the soluble normal form of prion protein can be transformed into an infectious misfolded conformation, PrP<sup>sc</sup>, having higher  $\beta$ -sheet content (Nyström and Hammarström, 2014; Prusiner et al., 1998). This infectious form can propagate by converting natively folded PrP into more PrP<sup>sc</sup>. Then, PrP<sup>sc</sup> aggregates

into amyloid fibers and kills neurons, leading to neurodegeneration (Brundin et al., 2010; Chaudhuri and Paul, 2006).

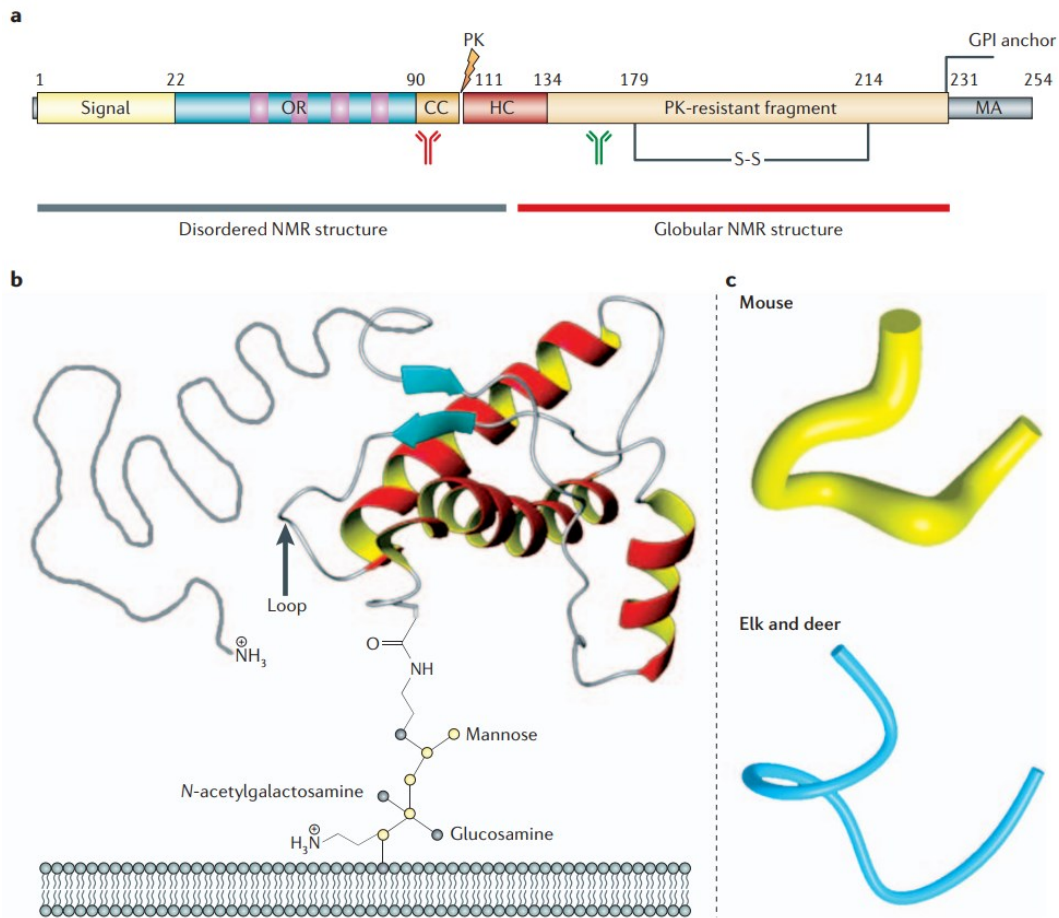


**Figure 1.7 The structures of the cellular prion protein (PrP<sup>c</sup>).** (a) The schematic of the prion protein (b) The tertiary structure of PrP from NMR spectroscopy includes the unstructured N-terminal (grey) and the GPI anchor that is inserted into a lipid bilayer. The black arrow indicates the loop region, which connects the second  $\beta$ -sheet and the third  $\alpha$ -helix structure. (c) The three-dimensional model of amino acids 165 to 172 of PrP, which is an extremely flexible loop in mouse PrP, yet almost entirely rigid in elk PrP and deer PrP.

Note: CC, HC, S-S and MA indicate the charged cluster, the hydrophobic core, the single disulfide bridge and the membrane anchor region, respectively, and the position of the amino acids are defined by the numbers on the top. The proteinase K (PK) resistant core of infectious prion protein (PrP<sup>Sc</sup>) and the approximate cutting site of PK are shown in gold color block and lightning symbol, respectively, reproduced from (Aguzzi and Heikenwalder, 2006).

Prion diseases or transmissible spongiform encephalopathies (TSEs) are a family of rare, progressive, infectious disorders in mammals, including bovine spongiform encephalopathy (BSE) or mad cow disease in cattle, chronic wasting disease (CWD) in deer and elk, scrapie in sheep and goats, and Creutzfeldt-Jacob disease (CJD) in humans (Collinge, 2001; 2016; Plummer, 1946).

**Table 1.4 Comparison of prion protein diseases**, adapted from (Aguzzi and Sigurdson, 2004; Hueston and Bryant, 2005; Prusiner et al., 1998).

Prion diseases	Scrapie (Sc)	Chronic wasting disease (CWD)	Bovine spongiform encephalopathy (BSE)	Variant Creutzfeldt-Jacob's disease (vCJD)
Host species	Sheep, goat	Mule deer, white-tailed deer, Rocky Mountain elk and moose	Cattle, ruminant	Humans
Date and place of the first recognition	1732, UK (identified retrospectively)	1967, USA (identified retrospectively)	1986, UK	1996, UK
Mechanism of transmission	Horizontal and possibly vertical transmission (Ingestion or contact infected animal or uptake from contaminated environment)		Ingestion of BSE-contaminated meat and bone meal	
Other susceptible species	Primates, hamsters, ovine PRNP (gene that encoded PrP)-transgenic mice and wild-type mice	Ferrets	Primates, bovine PRNP-transgenic mice, human PRNP-transgenic mice and wild-type mice	Human PRNP-transgenic mice and wild-type mice

Symptom	Slight behavior change (nervous, aggressive) followed by itching then motor abnormalities	Slight behavior change followed by repetitive behaviors, depression, then decreased appetite and then increased urination and stumbling	Slight behavior change (nervous, reluctant to enter doorways), teeth grinding and weight loss	Anxiety, depression, personality change followed by pain in limbs, face, body and then slurred speech, involuntary movement and memory loss
Duration of illness	1 to 6 months	2 to 3 months	1 to 3 months	12 to 18 months
Polymorphism codon(s) and code	136 A/V <sup>a</sup> 154 R/H 171 Q/R/H	White-tail deer: 95 Q/H, 96 G/S, 138 S/N Mule deer: 20 D/G, 225 S/F Elk: 132 M/L	50-91, with 5 or 6 octapeptide repeat in region	129 M/V

<sup>a</sup> Amino acid groups represent genotype combination (A = alanine, D = aspartate, G = glycine, H = histidine, K = lysine, L = leucine, M = methionine, N = asparagine, Q = glutamine, R = arginine, S = serine, V = valine)

According to previous studies of mutants of human prion protein, only a single amino acid difference can alter the protein enough to lead to disease (Asante et al., 2015; Mastrianni, 2010; Yin et al., 2007). Furthermore, the resistance to prion disease may be linked to the specific amino acid sequence of PrP within the host, as shown in table 1.4. For example, the polymorphisms in amino acids of sheep at codons 136, 154 and 171 are associated with scrapie susceptibility; for sheep that carry valine (V) at codon 136, they have higher susceptibility than those carrying alanine (A) (Goldmann et al., 1994).

The differences in the host PrP amino acid sequence also play an important role for the cross-species transmission of prion diseases (Cassard et al., 2014). Some animals expressing same amino acid residue at the position 170 were surprisingly found to have different susceptibility (Table 1.5). For example, both squirrel monkeys and macaques have asparagine (N) at codon 170; squirrel monkeys were highly susceptible to CWD prion infection, whereas macaques were resistant to the disease. Furthermore, a comparison of the prion protein amino acid sequences of both animals indicated that there are 2 amino acid differences at position 100 and 108, which may impact resistance to CWD; the sequence alignment of prion proteins from different species is shown in figure 1.8. Nonetheless, the underlying structural mechanism resulting in the differences in CWD susceptibility is not clearly identified (Kurt and Sigurdson, 2016).

**Table 1.5 Species susceptibility to Chronic wasting disease (CWD) infection,** adapted from (Kurt and Sigurdson, 2016).

Species	Amino acid (position 170)	Percentage of CWD infection via the intracerebral routes of exposure
White-tailed deer	N	75-100%
Prairie vole, Meadow vole, Bank vole	N	75-100%
Chinese hamster	N	25-74%
Armenian hamster, Syrian golden hamster, Siberian hamster	N	0-24%
Djungarian hamster	N	0%
Transgenic mice expressing hamster PrP	N	25-74%
Deer mouse, white-footed mouse	N	25-74%



for example, mice have a lower susceptibility to prion disease than hamsters, yet a higher susceptibility than rabbits (Fernandez-Funez et al., 2011; Nyström and Hammarström, 2014). Therefore, the small changes in the amino acid sequence may be very important to shed more light on the differences in the susceptibility to prion disease of different species.

This work aimed to use single molecule experiments to better understand the folding of mouse PrP, a model system for studying prion diseases. Measurements of single mouse PrP molecules, which mechanically unfolded and refolded by laser tweezers, were made in order to compare to the previous single-molecule studies of hamster prion proteins and search for any commonalities or differences in the folding and unfolding behavior between the species. The eventual goal was to connect the sequence differences and folding behavior to obtain new insight into disease susceptibility in the future.

## **1.4. Outline of the Rest of Thesis**

The main objective of this thesis is to investigate the information from the mouse prion protein obtained using single-molecule force spectroscopy in order to be able to compare the folding behavior of the prion protein from different species in the future. This thesis is divided into five chapters, in which the second chapter presents optical tweezers, the single-molecule study method for the prion protein in this study, including the proper way to analyze data obtained from the relationship between applied forces and the protein extensions. The third chapter describes the preparation of mouse prion protein samples, DNA handles, and protein-handle attachments, including the verification of successful attachments. The fourth chapter consists of the results from the optical tweezers measurements of both handle-handle attachments and protein-handle attachments, as well as the analysis of the contour length changes in the protein during unfolding/refolding and the comparison of force-extension curves from PrP from different species. Finally, several ideas for possible future work are suggested in the fifth chapter of this thesis.

## **2. Single-Molecule Force Spectroscopy Studies**

### **2.1. Optical Tweezers**

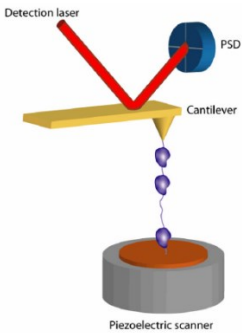
In the past two decades, many mechanical manipulation methods have been invented for nano-scale observations of biological molecules, such as Atomic Force Microscope (AFM), Acoustic Force Spectroscopy (AFS), Biomembrane Force Probe (BFP), Glass Microneedles, Magnetic Tweezers, Nanopore and Optical Tweezers (as shown in table 2.1).

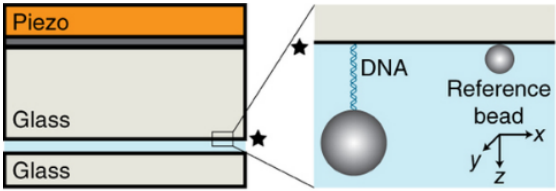
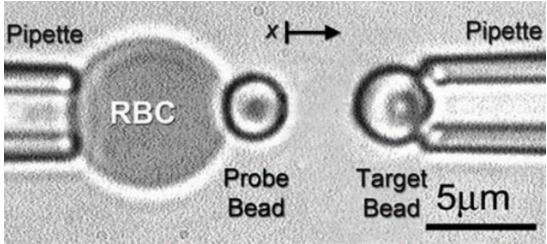
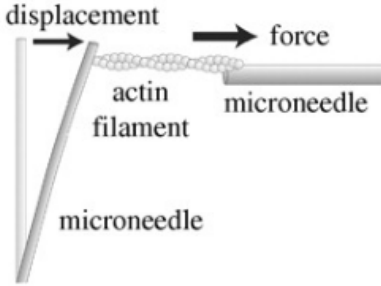
Nowadays, the understanding of the mechanism of prion misfolding and propagation, including the effective ways of treating prion diseases, is not clearly identified. Nano-scale manipulation methods can be used as a new tool to better comprehend the mechanisms and dynamics of protein misfolding. In this study, optical tweezers were used in order to manipulate the protein by grabbing onto beads attached to the molecule. Micron-sized dielectric particles like plastic beads can be trapped by a focussed laser beam because of the force generated by the electric field intensity gradient of a laser on the dipole induced in the dielectric, as shown in figure 2.1 (Ashkin, 1986). Translation of the laser beam by optical elements like mirrors and deflectors then allows the position of the beads to be manipulated precisely. The gradient force in the trap acts like a restoring force, allowing the force acting on the bead to be determined from Hooke's law by measuring the displacement of the bead from the centre of the trap. The principles of optical trapping and how they can be implemented in experiments are described in several review papers (Bustamante et al., 2009; Neuman and Block,

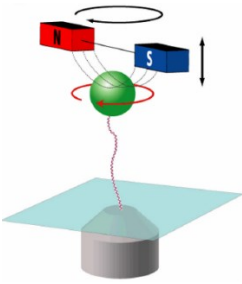
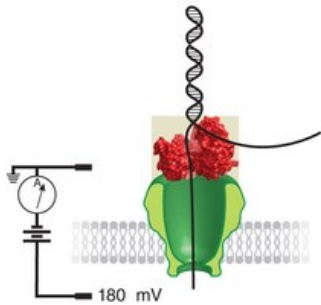
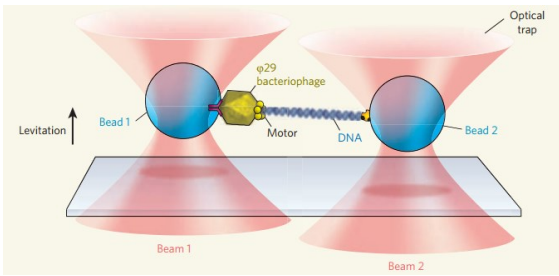
2004). The construction of the instrument used in this work was described previously by Daniel Foster (Foster, 2010).

In 1987, the ability of optical tweezers to manipulate living cells without damage was first demonstrated by trapping living bacteria and virus (Ashkin et al., 1987; Pool, 1988). Since then, optical tweezers have been used in numerous biology applications, such as the dynamics of motor proteins (myosin walking along actin filaments, kinesin and dynein walking on a microtubules) and intracellular materials, namely, chloroplasts and chromosomes (Bayouth et al., 2001; Berns et al., 1989; Shingyoji et al., 1998; Svoboda et al., 1993). Furthermore, optical tweezers have been used for the study of the stretching and folding of proteins or nucleic acids (Cecconi et al., 2005; Liphardt et al., 2001; Perkins et al., 1994; Ritchie et al., 2015).

**Table 2.1. The methods for the mechanical manipulation of single molecules by stretching of the molecules in elongation flow**

Method	Principle	Examples
Atomic Force Microscope (AFM)	 <p>The sample is attached to the cantilever tip and surfaced on the piezo stage, which is retracted along the axial direction, resulting in the molecule extension.</p>	Ligands-receptors interaction and unfolding of a single protein or poly-protein molecule (Carrion-Vazquez et al., 1999; Moy et al., 1994; Neuman and Nagy, 2008)

<p>Acoustic Force Spectroscopy (AFS)</p>	 <p>The tethers between a surface and microsphere are stretched by the acoustic force.</p>	<p>DNA overstretching and mechanical unfolding of protein in parallel. (Kamsma et al., 2016; Sitters et al., 2015)</p>
<p>Biomembrane Force Probe (BFP)</p>	 <p>A left micropipette-aspirated sample with a bead is held stationary, and the right pipette consisting of another bead is moved in a repeated cycle.</p>	<p>Red blood cell (RBC) and T cell adhesion and molecular adhesion and activation of cytoskeletal structure (Evan et al., 1995)</p>
<p>Glass Microneedles</p>	 <p>The filament bound to a flexible glass needle is stretched through a stiff needle that is bound at another end.</p>	<p>Single actin filament and actin-myosin interaction (Kishino and Yanagida, 1988; Ishijima et al., 1996)</p>

<p style="writing-mode: vertical-rl; transform: rotate(180deg);">Magnetic Tweezers</p>	 <p>Magnetic field gradient is produced by permanent magnets resulting in a force on the bead.</p>	<p>Single molecule of DNA, DNA-binding protein and receptor-ligand interactions (Danilowicz et al., 2005; Neuman and Nagy, 2008)</p>
<p style="writing-mode: vertical-rl; transform: rotate(180deg);">Nanopore</p>	 <p>The charged polymer is driven by using an electric field.</p>	<p>Unzipping of DNA hairpin and DNA-protein interaction (Deamer et al., 2016; Dudko et al., 2010; Petrosyan et al., 2015)</p>
<p style="writing-mode: vertical-rl; transform: rotate(180deg);">Optical Tweezers</p>	 <p>The molecule is attached to the beads manipulated by strongly focused laser beams</p>	<p>Organelles in living cells and DNA translocation (Abbondanzieri and Zhuang, 2009; Norregaard et al., 2017)</p>

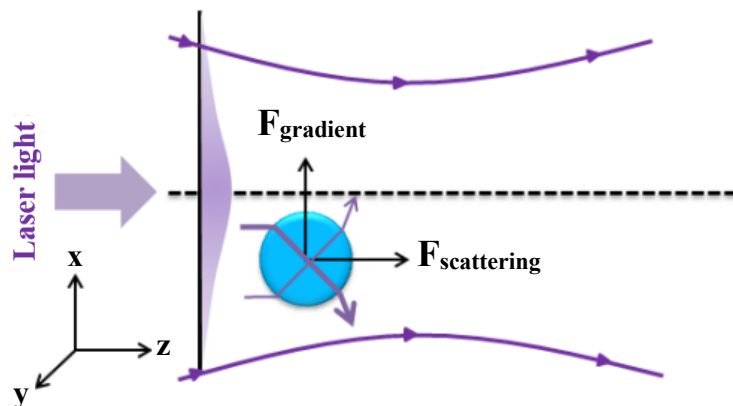


**Figure 2.1 Optical tweezers diagram.** The single beam having a Gaussian intensity profile was created using high numerical aperture converging lens. The effect of the forces results in the stable trap at the focal point of the laser beam.

The single-trap design is the simplest optical tweezers setup (figure 2.2). The protein is attached to two beads, of which one is trapped in a laser beam, and another is held by a micropipette. However, the stability of optical tweezers can be increased by using the dual optical trap setup (Meiners and Quake, 1999; Abbondanzieri et al., 2005). Thus, in the experiments described in this thesis, the mouse prion protein is attached to DNA handles at both ends, and then the protein-DNA handle construct is tethered to two beads that are manipulated by using a dual-trap optical tweezers setup, as shown in figure 2.3.

The main reason why the protein molecules have to be attached to tethers (handles) in the dual-trap optical tweezers is because the beads have to be far enough apart in order to avoid interference between the two trapping potentials, and also to reduce hydrodynamic coupling between the beads. During the manipulation, forces are measured from the displacement of the bead out of the trap centre, and extensions of the protein-handle constructs are measured from the distance between the two beads.

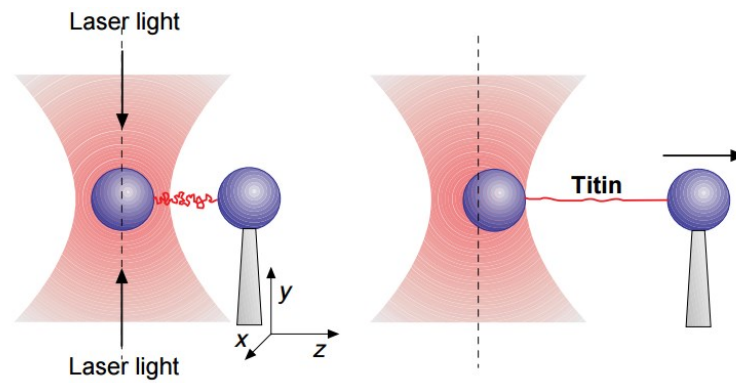


**Figure 2.2 Single-beam optical tweezers apparatus.** The giant filamentous polypeptide (Titin) was attached between two beads. In order to stretch the molecule, the micropipette was moved away from the optical trap (z direction), reproduced from (Kellermayer et al., 1997).

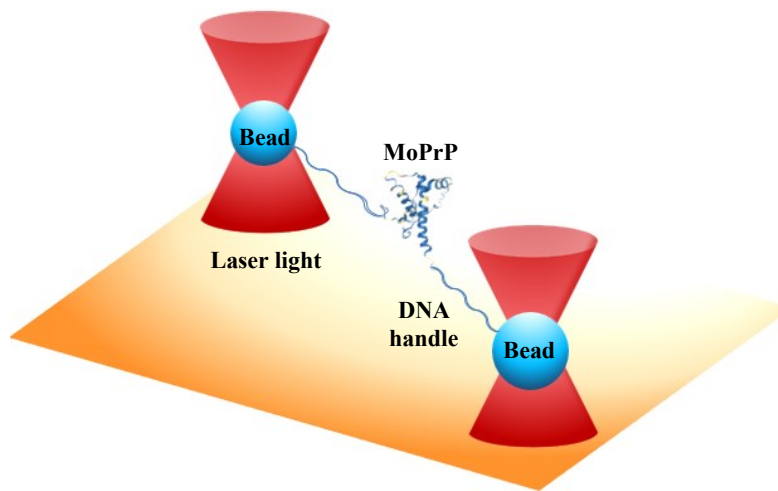


**Figure 2.3 Schematic of the dual-beam optical tweezers for the prion protein stretching experiment.** The mouse prion protein (MoPrP) was tethered between two beads for the single-molecule study.

## 2.2. Data Analysis

When pulling on a single molecule (whether tethers plus protein or just DNA handles alone), the force increases as a function of extension resulting in a typical shape for the pulling curves, as shown in figure 2.4. In order to describe the mechanical properties in single molecule experiments, the molecule can be modelled as a flexible rod. Thus, the force-extension curves of the sample can be fitted by using the wormlike chain (WLC) model, a model of polymer elasticity, yielding the contour length of the sample ( $L_c$ ) (Guo et al., 2013; Janshoff et al., 2000).

The WLC model was firstly treated by Fixman and Kovac in 1973, and then Kovac and Crabb performed the analytical approach in 1982 (Bouchiat et al., 1999). The WLC model was then developed by Marko and Siggia and reported by Bustamante for studying DNA stretching in 1994 (Bustamante et al., 1994; Bouchiat et al., 1999).

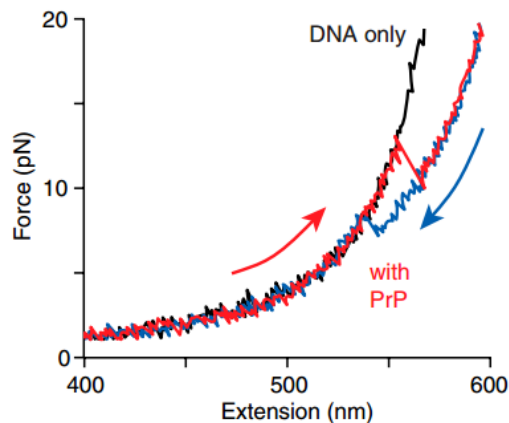


**Figure 2.4 Force-extension curve of the protein-DNA handle attachment and the DNA handles.** Stretching (red) and refolding (blue) force-extension curve of protein indicated the two-state behavior compared to the one state behavior of the DNA handles alone (black), reproduced from (Yu et al., 2012).

After that, this model was also used for the description of the mechanical unfolding of proteins (Carrion-Vazquez, 1999). The relationship between force and extension in this experiment can be interpreted by using the modified Marko-Siggia WLC model according to the following equation (Marko and Siggia, 1995; Wang et al., 1997)

$$F(x) = \left( \frac{k_b T}{L_p} \right) \left[ \frac{1}{4 \left( 1 - \frac{x}{L_c} + \frac{F}{K} \right)^2} - \frac{1}{4} + \frac{x}{L_c} - \frac{F}{K} \right] \quad (2.1)$$

Here  $x$  is the extension (end-to-end distance),  $F(x)$  is the applied force as a function of extension,  $L_p$  is the persistence length of the chain (related to the polymer's flexibility),  $L_c$  is the contour length of the chain (the total length along the backbone),  $K$  is the elastic modulus (the resistance of the polymer to the longitudinal stretching) and  $k_b T$  is the Boltzmann constant times absolute temperature. For folding studies,  $L_c$  is especially important, because a molecule becomes longer when its structure unfolds, as seen in the “rip” in the curves in Figure 2.5.

In this experiment, the prion protein was attached to DNA handles at both ends, and the force-extension curves were analyzed by using two WLC models in series, consisting of one WLC model for the DNA handle and a second WLC model for the protein. At low forces, where the protein was folded, the force-extension curve (FEC) represented the extension of the DNA handle only. Thus, the FECs were first fit at low force using the WLC parameters of the DNA handle. The persistence length of the double stranded DNA (dsDNA) handles was in the range of 30 to 50 nm, with a mean value of 35 nm, the contour length for dsDNA determined by X-ray crystallography is 0.34 nm per nucleotide, and the elastic

modulus for dsDNA was found previously to be 1000-1500 pN (Brinkers et al., 2009; Wang et al., 1997).

Next, the part of the FECs after the unfolding rip were fitted by using the parameters for the handle as at low force, but adding in a second WLC to represent the protein. The persistence length of proteins is usually on the order of 0.6-0.8 nm and the approximate contour length for a protein molecule is 0.36 nm per amino acid (Stirnemann et al., 2013). From the change in contour upon unfolding, we can therefore determine the number of amino acids unfolded in the protein. By comparing this number to the known length of the protein, we can then determine if the protein was folded correctly or misfolded.

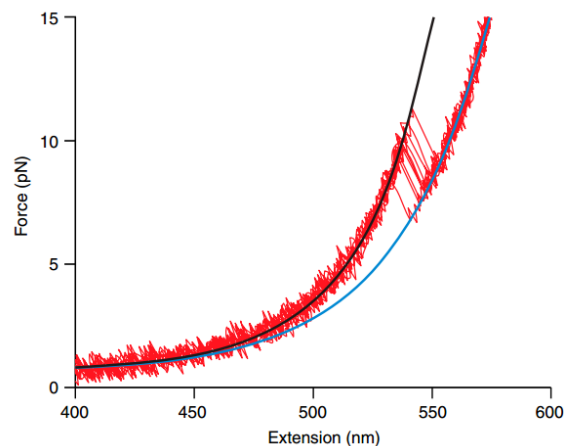


**Figure 2.5 Ten unfolding force-extension curves of protein (red traces) fitting to the WLC model.** The black and blue traces show the WLC fit to the folded and unfolded states, respectively. The force-extension curves were fitted at low force using the WLC parameters of the flexible DNA handle alone; these parameters include persistence length ( $\sim 35$  nm), contour length (0.34 nm per base pair), and elastic modulus (1000-1500 pN). The WLC parameters for the unfolded protein at high force were persistence length (0.65 nm), contour length (0.36 nm per amino acid), and elastic modulus (2000 pN). Reproduced from (Yu et al., 2012).

## **3. Sample Preparation**

### **3.1 Prion Protein Expression and Purification**

In order to perform single-molecule force spectroscopy of mouse prion protein (MoPrP) attached to DNA handles, the protein was engineered to have one cysteine at both the N terminus and C terminus, for specific labelling with tetrazine (tz). The prion protein was expressed and purified by Craig Garen, a technician in the Woodside Lab, by the following procedures.

#### **3.1.1. The expression of prion protein**

First of all, the recombinant prion protein expressed in a single colony of *E. cloni*® EXPRESS BL21 from the Lucigen Corporation was inoculated into 5 ml of Luria-Bertani (LB) media containing 100 µg/ml of ampicillin and incubated at 37°C overnight in a shaking incubator. After the overnight incubation, the culture was inoculated into 1 L of LB with 100 µg/ml of ampicillin (pre-warm media at 37°C) and incubated until the optical density of the sample, from the UV spectroscopy measured at a wavelength of 600 nm ( $OD_{600}$ ), reached approximately 0.6. Then, in order to induce the expression, isopropyl β-D-1-thiogalactopyranoside (IPTG) was added to a final concentration of 1.0 mM, and then the sample was incubated for 3 to 4 hours at 37°C with shaking. After that, the cells were harvested by centrifugation at 6000 x g for 20 minutes at 4°C. The cell pellets were washed with Phosphate-buffered saline (PBS), includes 137 mM of sodium chloride (NaCl), 2.7 mM of potassium chloride (KCl), 10 mM of disodium hydrogen

phosphate ( $\text{Na}_2\text{HPO}_4$ ) and 1.8 mM of monopotassium phosphate ( $\text{KH}_2\text{PO}_4$ ), pH 7.4, and stored at  $-80^\circ\text{C}$ .

### **3.1.2. The purification of prion protein**

The frozen cell pellet was resuspended in 25 ml of the Lysis Buffer (6 M of guanidine hydrochloride (GdnHCl), 50 mM of monosodium phosphate ( $\text{NaH}_2\text{PO}_4$ ), 500 mM of NaCl, 0.5 mM of phenylmethane sulfonyl fluoride (PMSF) and 20 mM of imidazole, pH 7.4) at room temperature and sonicated in an ice bucket three times for 10 seconds at 50% and 10 seconds intervals. After the sonification, beta-mercaptoethanol ( $\beta$ ME) was added to the final concentration of 10 mM, followed by the addition of Tween™ 20 (Product Code: BP337500) from the Fisher BioReagents™ to the final concentration of 0.5%. The cell lysate was then transferred into a 50 ml falcon tube and centrifuged at 12,000 relative centrifugal force (rcf) for 40 min at  $4^\circ\text{C}$ , in order to create pellet cellular debris. After that, the sample was filtered using a 0.45  $\mu\text{m}$  pore size syringe filter (30 mm diameter, Product Code: 229749) from the CELLTREAT® Scientific Products and purified at  $4^\circ\text{C}$  using liquid chromatography systems by loading the solution onto a Ni-NTA Superflow Cartridge (5 x 5 ml, Product Code: 30761) from the QIAGEN. The column was washed with the Lysis Buffer until the absorbance at 280 nm ( $A_{280}$ ) returned to the background level. Then, the prion protein was eluted from the column by applying the Elution Buffer (6 M of GdnHCl, 50 mM of phosphate buffer and 250 mM of imidazole, pH 7.4).

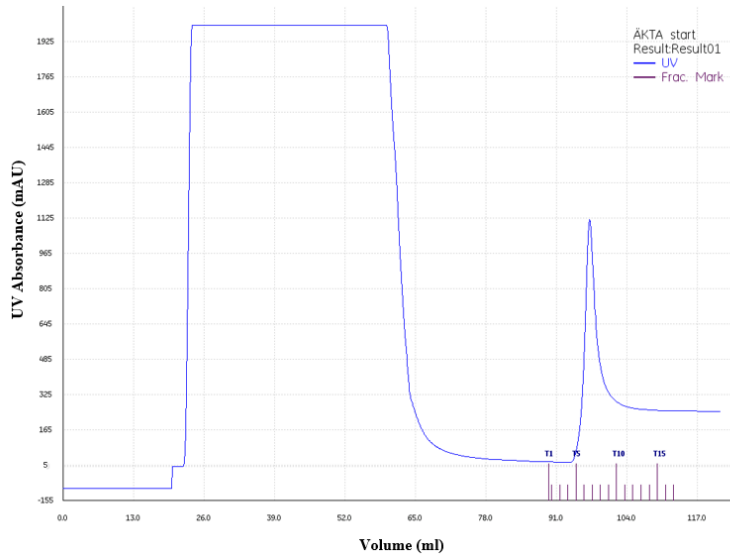


**Figure 3.1 Representative elution profile of the mouse prion protein (MoPrP) purification on the column from Craig Garen.**

### **3.1.3. The refolding of prion protein**

In order to make sure that the properly folded protein was produced, the prion protein after the purification was refolded in the refolding buffer, by the following procedures. First of all, the purity and identity of the prion protein in each eluted fraction can be identified using the sodium dodecyl sulphate-polyacrylamide gel electrophoresis (SDS-PAGE) analysis. The separating gel was made by mixing the gel solution (3.6 ml of water, 2.5 ml of 1.5 M trisaminomethane (Tris), pH 6.8, 3.75 ml of 40% acrylamide, 100  $\mu$ l of 10% sodium dodecyl sulphate (SDS), 50  $\mu$ l of 10% Ammonium persulfate (APS) and 5  $\mu$ l of Thermo Scientific Pierce Tetramethylethylenediamine (TEMED, Product Code: 17919) from the Thermo Scientific™). After that, the solution was stirred thoroughly and pipetted into the gap between the glass plate of the casting frames. The top of the separating gel was then filled with 70% ethanol in order to make space for

the stacking gel. Then, the stacking gel was made by gently mixing the gel solution (3.8 ml of water, 0.63 ml of 1.0 M Tris, pH 6.8, 0.5 ml of 40% acrylamide, 50  $\mu$ l of 10% SDS, 25  $\mu$ l of 10% APS and 5  $\mu$ l of TEMED). After the separating gel was polymerized for 30 minutes, the 70% ethanol on the top of the gel was discarded. The mixture of the stacking gel was then pipetted into the top of the gap between the glass plate, followed by insertion of the well-forming comb. The stacking gel should be polymerized within approximately 30 minutes. After that, the electrophoresis buffer was then poured until reaching the required level in the outer chamber. In order to analyze the mouse prion protein fractions in SDS-PAGE, the prepared sample was heated in boiling water at 75°C for 10 minutes and then loaded into the wells in the gel. The top of the chamber was covered, connected to the power supply, and the sample was undergone electrophoresis according to the conditions at 110 volts (V) for 30 minutes followed by 160 V for 75 minutes. After the electrophoresis was completed, the power supply was turned off. Next, the gel was removed from the cassettes, stained using Bio-Safe™ Coomassie Stain and placed on the shaker overnight. Finally, the gel was transferred into another plastic box and rinsed with water before imaging.

The protein in the fractions of interest was titrated into the refolding buffer (1.1 M GdnHCl, 55 mM Tris, 21 mM NaCl, 0.8 mM KCl, 1 mM L-Glutathione reduced (GSH, Product code: G4251) from the Sigma-Aldrich® and 1 mM Glutathione oxidized (GSSG, Product code: 3542) from the Calbiochem®, pH 8.2) at a final dilution factor of 1:10 (protein: refolding buffer). The solution was stirred and stored overnight at 4°C. After that, the refolded protein was dialyzed against

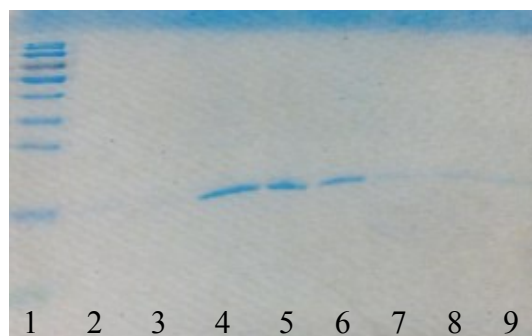


**Figure 3.2 Analysis of mouse prion protein fractions in SDS-PAGE.** The band for the protein of interest becomes more prominent than the other bands. Note: Lane 1 is the protein ladder and lanes 2-9 are the mouse prion protein from the A3-A10 fractions, respectively.

H<sub>2</sub>O overnight at 4°C. In order to check the protein concentration before the lyophilisation or freeze-drying, the concentration of the protein solution was measured with the absorbance curve at a wavelength of 280 nm ( $A_{280}$ ) using Ultraviolet–visible spectroscopy (UV-Vis) and was then aliquoted into 50 ml tubes. Each tube was flash-frozen in liquid nitrogen, covered with KIMTECH SCIENCE KIMWIPE Dedicare Task Wipers (Product Code: 34120) from Kimberly-Clark PROFESSIONAL, placed in a freeze-drying flask of the FreeZone Plus 2.5 Liter Cascade Benchtop Freeze Dry System (Product Code: 7670020) from the LABCONCO® for 2 to 3 days and then stored at -80°C. Before the labelling with tetrazine, the secondary structural composition of the prion protein after the refolding procedure can be checked by using Circular dichroism (CD) spectroscopy.

### 3.1.4. Circular dichroism spectra of prion protein

Circular dichroism spectroscopy is the most commonly used technique to estimate the secondary structural composition of a protein by analyzing the differential absorption of the two types of circularly polarized light by a number of chromophores (peptide bond, aromatic side chain and disulfide bond) in protein (Kelly and Price., 2000; Micsonai et al., 2015). Each type of secondary structure in proteins has a characteristic shape of the CD spectrum as shown in figure 3.3. An alpha-helical protein has a positive absorbance peak at 193 nm and negative absorbance peaks at 208 and 222 nm, whereas a beta-sheet protein has a positive absorbance peaks at 208 and 222 nm, whereas a beta-sheet protein has a positive absorbance peak at 195 nm and a negative absorbance peak at 218 nm (Greenfield and Fasman, 1969; Holzwarth and Doty, 1965).

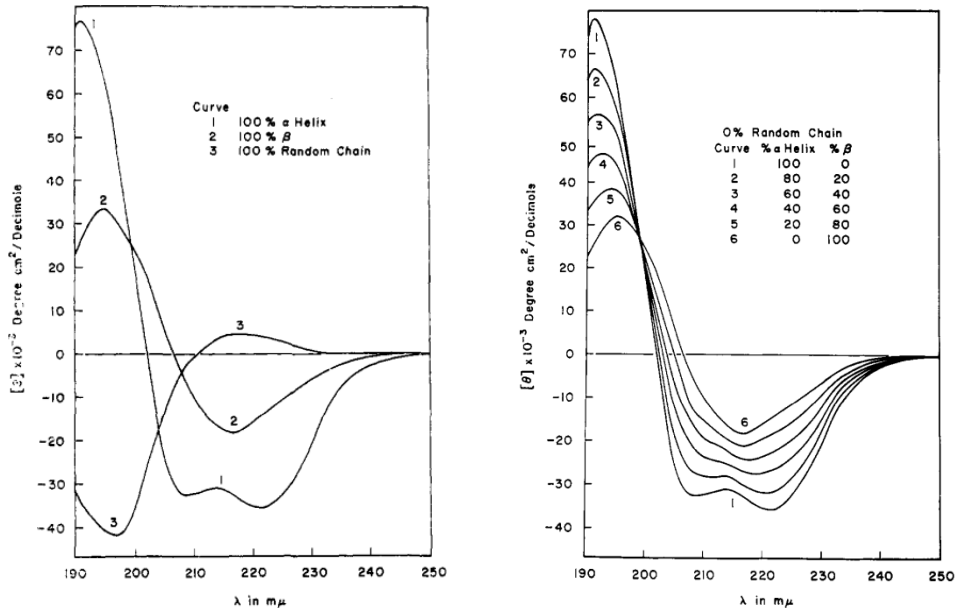


**Figure 3.3 CD Spectra of poly-L-lysine**, reproduced from (Greenfield and Fasman, 1969). (a) The poly-L-lysine in alpha helix, beta sheet and random coil structure. (b) The poly-L-lysine contained 0% random coil and different percentages of alpha helix and beta sheet structure.

In this experiment, the prion protein was diluted to the final concentration of 5  $\mu\text{M}$  with 400  $\mu\text{l}$  of the 30 mM of sodium acetate (NaOAc), and then the CD spectra was measured using the Jasco J-810 Spectrometer. During the first period of this experiment, the mouse prion protein labelled with tetrazine could not attach to the DNA handle successfully. After the problem was solved, I found that there was a difference between the CD spectra of the mouse prion protein that successfully attached to the DNA handle and of the mouse prion protein that unsuccessfully attached to the handle. Thus, in order to make sure that the properly folded protein was produced before labelling with tetrazine, the secondary structural composition of the fresh prion protein, after the purification, was checked by using CD Spectroscopy before the labelling.

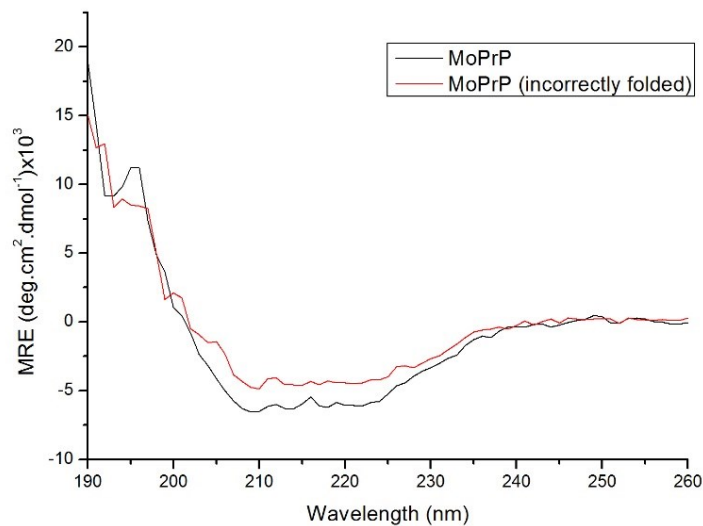


**Figure 3.4 Comparison between the CD Spectrum of mouse prion protein that successfully attached to the DNA and unsuccessfully attached to the handle.** CD spectrum of the problem mouse prion protein shows different content compared with the mouse prion protein that was attached to the DNA handle successfully.

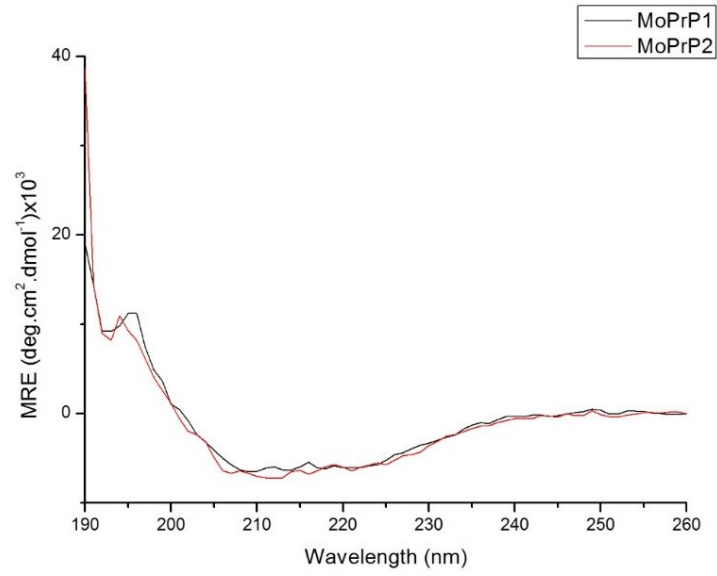


**Figure 3.5 Representative CD Spectra of mouse prion protein after the refolding procedure.** In order to make sure that the mouse prion protein was folded properly, the new mouse prion protein after the purification was measured the CD Spectrum using the spectrometer.

## 3.2 Protein Labelling

### 3.2.1. Prion protein labelling with tetrazine

Since proteins contains various amino acids, methods for selective chemical labelling of protein have been developed to achieve highly efficient labelling (Chen and Wu, 2016; Devaraj et al., 2009; Devaraj and Weissleder, 2011). In 2008, there was the first report on the reaction between a strained molecule transcyclooctene (TCO) and a tetrazine (tz) compound (Blackman et al., 2008). Since the rate of tetrazine-cycloaddition transformation was reported, this reaction has been found to be faster than most other biorthogonal reactions and this bioconjugation has been used in a variety of biological applications (Devaraj et al., 2008; 2012; Lang et al., 2012; Rossin et al., 2013; Selvaraj and Fox, 2013).

In this experiment, the prion protein was labelled with tetrazine in order to attach to TCO-functionalized DNA handles for the single-molecule study of the protein. The protein sample stored at  $-80^{\circ}\text{C}$  was mixed with 10 ml of 30 mM of NaOAc (pH 4.6) at room temperature and run through 10 kDa molecular weight cut-off (10 kDa MWCO) Amicon spin filter using centrifugation at 4000 rcf for 20 minutes. After that, the mixture was rinsed and spun down at least 3 times to achieve an approximate final volume of 500  $\mu\text{l}$ . Then, the sample was moved to a new vial and the concentration of the protein was checked by measuring the absorbance curve at a wavelength of 280 nm ( $A_{280}$ ) using UV-Vis.

In order to label the prion protein using tetrazine, the protein was reduced with cysteamine hydrochloride (MEA, Product Code: M6500-25G) from the Sigma-Aldrich®. The protein was mixed in 200 µl of sodium dihydrogen phosphate buffer (150 mM of NaH<sub>2</sub>PO<sub>4</sub> and 30 mM of Ethylenediaminetetraacetic acid (EDTA)), 200 µl of MEA solution (85 mg of EDTA in 5 ml of the NaH<sub>2</sub>PO<sub>4</sub> buffer), and water to achieve a final prion protein concentration of 14-15 µM in 600 µl of the mixture; the solution was incubated for 45 minutes at room temperature. Then, in order to get rid of the excess MEA, the mixture was run through 10 kDa MWCO Amicon spin filter using centrifugation at 4000 rcf for 15 minutes. The protein solution was rinsed and spun through the spin filter at least 2 times. After that, 10 µl of 40 mM tetrazine dissolved in Dimethyl Sulfoxide Hybri-Max™ (DMSO, Product Code: D2650) from the Sigma-Aldrich® was added to the mixture and incubated for 1 hour at room temperature.

Next, the protein solution was diluted to 1 ml by adding 500 mM of NaOAc and run through 10 kDa MWCO Amicon spin filter using centrifugation at 14000 revolutions per minute (rpm) for 4.5 minutes. The mixture was rinsed and spun down at least 3 times to reduce the excess tetrazine. Finally, the concentration of the protein labelled with tetrazine was measured with the absorbance curve at the wavelength of 280 nm using the NanoDrop from Thermo Fisher Scientific Inc.

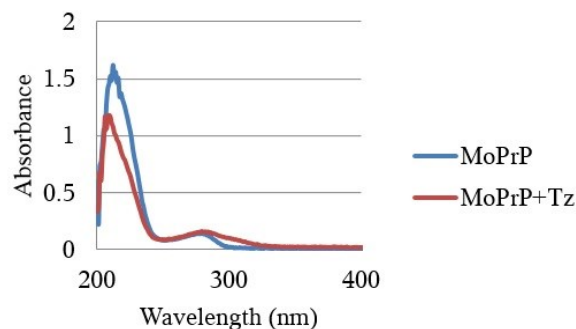


**Figure 3.6 The ultraviolet absorption of mouse prion protein (MoPrP) and Mouse Prion Protein labelled with tetrazine (MoPrP+Tz)** The concentration of protein can be obtained by using the value of absorbance of protein at 280 nm. Furthermore, the absorbance curves at around 300 nm showed the difference between prion protein alone and prion protein labelled with tetrazine.

The quality of the protein labelled with tetrazine was checked by using the TCO-activated Cyanine5 (Cy5) probe (Cy5-TCO, Product Code: 1089) from the Click Chemistry Tools according to the following procedures. The prion protein and the tetrazine modified prion protein were mixed with 250  $\mu\text{M}$  of Cy5-TCO to the final concentration of 140  $\mu\text{M}$  of Cy5-TCO and 80  $\mu\text{M}$  of prion protein in 15  $\mu\text{l}$  of the solution. Then, mixtures were incubated at room temperature for 2 hours, heated in boiling water at 75°C for 10 minutes and loaded into the wells of the SDS-PAGE gel. The gel was undergone electrophoresis according to the conditions at 110 V for 30 minutes followed by 160 V for 75 minutes. After the electrophoresis was completed, the SDS-PAGE gel was removed from the cassettes, rinsed with water, and the fluorescent image was taken. Finally, the gel was stained using Bio-Safe™ Coomassie Stain, placed on the shaker overnight, rinsed with water and another image was taken using camera.

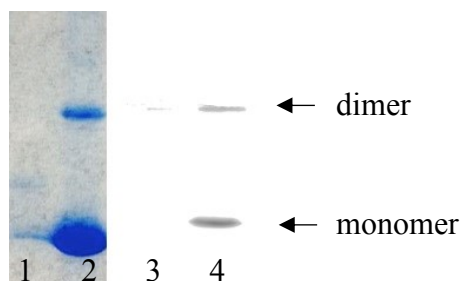


**Figure 3.7 SDS-PAGE Analysis of mouse prion protein and Cy5-TCO.** The tetrazine modified mouse prion protein mixed with Cy5-TCO can be visualized by using the fluorescent image analyzer. Note: Lane 1 and lane 2 are the image of SDS-PAGE gel of the mouse prion protein with Cy5-TCO and the tetrazine modified mouse prion protein with Cy5-TCO, respectively. Lane 3 and lane 4 are the fluorescent image of the wild-type mouse prion protein with Cy5-TCO and the tetrazine modified mouse prion protein with Cy5-TCO, respectively.

### 3.2.2. Problem with the internal cysteine of prion protein

The mouse prion protein (MoPrP) was engineered to have one cysteine at each terminus for the specific labelling with tetrazine, but there were also two internal cysteine residues already present in the sequence of the mouse prion protein, as shown in the figure 3.8. In order to make sure that the tetrazine was reacting only with the cysteines at the ends (for attachment to the DNA handles), this experiment was conducted by Derek Dee according to the following procedures.

```

90  GQGGGTHNQW  NKPSKPKTNL  KHVAGAAAAG  AVVGGGLGGYM  LGSAMSRPMI
                                     ....β1....

140  HFGNDWEDRY  YRENMYRYPN  OVYYRPVDOYS  NONNFVHDCY  NITIKOHTVT
      .....α1.....          ...β2...          .....α2.....

190  TTTKGENFTE  TDVKMMERVV  EQMCVTQYQK  ESQAYYDGRR  S
      .....          .....α3.....

```

**Figure 3.8 Sequence of the wild type mouse prion protein.** The residues highlighted in green represent important residues that define the species barriers between hamsters and mice.

In order to make the comparison between the tetrazine labelling at only both ends of the mouse prion protein at the cysteine modified residue and the tetrazine labelling at the internal cysteine, two types of the mouse prion protein were used in this experiment: the mouse prion protein that was specially engineered to have the cysteines the both ends (2Cys-MoPrP) and the normal mouse prion protein or the “wild-type” mouse prion protein (WT-MoPrP).

First, the 2Cys-MoPrP and the WT-MoPrP in the sodium acetate solution were mixed with 200  $\mu$ M of the tris(2-carboxyethyl)phosphine (TCEP, pH 6.8) and incubated for 1 hour at room temperature to reduce disulfide bonds in the prion protein for the tetrazine labelling. Next, 400  $\mu$ M of the maleimide - polyethylene glycol 4 - tetrazine (mal-PEG4-Tz) was added into the mixture and then incubated for another 2 hours at room temperature. After the incubation, the solution was run through 10 kDa MWCO Amicon Spin Filter using centrifugation to get rid of the excess tetrazine. In order to check the specific labelled residue with tetrazine, both prion proteins labelling with tetrazine were mixed with Cy5-TCO, incubated at room temperature for 2 hours, heated and loaded into the wells of the SDS-PAGE gel. After the electrophoresis was completed, the gel was rinsed with water, and the fluorescent image was taken. Finally, the gel was stained using Bio-Safe™ Coomassie Stain, placed on the shaker overnight, rinsed with water and another image was taken using a camera.

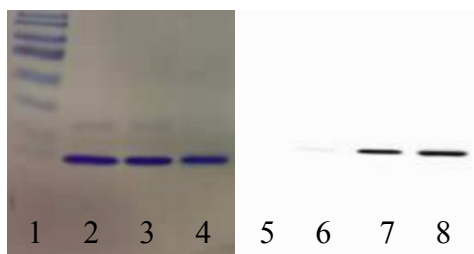


**Figure 3.9 SDS-PAGE Analysis of mouse prion protein labelled with tetrazine using TCEP and Cy5-TCO from Derek Dee.** The tetrazine labelling of modified mouse prion protein (2Cys-MoPrP) and wild type mouse prion protein (WT-MoPrP) mixed with Cy5-TCO could be able to visualize by using the fluorescent image analyzer because of the labelling at the internal cysteine residue. Note: Lanes 1-4 are the image of SDS-PAGE gel and lanes 5-8 are the fluorescent image, respectively. Lanes 1 and 5 are the protein ladder, lanes 2 and 6 are the WT-MoPrP and Cy5-TCO, lanes 3 and 7 are the WT-MoPrP labelled with tetrazine by using TCEP and Cy5-TCO, and lanes 4 and 8 are the 2Cys-MoPrP labelled with tetrazine by using TCEP and Cy5-TCO.

According to the fluorescent image analyzer of the SDS-PAGE gel, the cysteine residues of both mouse prion proteins were labelled with tetrazine resulting from the tetrazine labelling at the internal cysteine residue of both prion protein samples. However, in order to study the single-molecule force spectroscopy of the total length of this prion protein sample, the tetrazine should be labelled at only both cysteine residues at the end of the mouse prion protein of the 2Cys-MoPrP for the attachment to the DNA handle.

The problem of the internal cysteine labelling with tetrazine was also solved by Derek Dee by using MEA, the milder reductant for the reduction of the disulfide bonds in the prion protein, instead of using the stronger reductant (TCEP) in the labelled reaction (Makaraviciute et al., 2016). Both 2Cys-MoPrP and WT-MoPrP in the sodium acetate solution were mixed with different concentration of MEA (5  $\mu$ M, 10  $\mu$ M, and 50  $\mu$ M), incubated for 45 minutes at room temperature

and then centrifuged to get rid of the excess MEA. Next, the solution was mixed with tetrazine and incubated for 1 hour at room temperature. After the mixture was spun down to reduce the excess tetrazine, the Cy5-TCO was added to the solution. The sample was incubated, heated and put through electrophoresis; both the fluorescent image and the image after staining with Coomassie blue were taken as same as the previous procedures. The fluorescent image analyzer of the SDS-PAGE gel indicated that only cysteine residues at both ends of the 2Cys-MoPrP were labelled with tetrazine by using MEA at the concentration of 10  $\mu$ M and 50  $\mu$ M. Thus, in order to label the tetrazine, MEA is the better reductant to use in this experiment for the protein attachment to the DNA handle at the end of the prion protein for the single-molecule study.

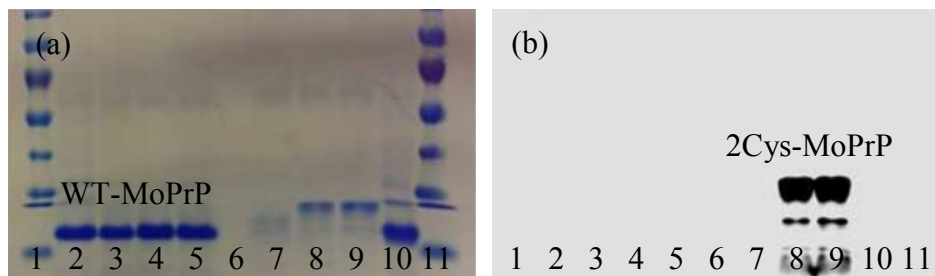


**Figure 3.10 SDS-PAGE Analysis of mouse prion protein labelled with tetrazine using MEA and Cy5-TCO from Derek Dee.** Only the modified mouse prion protein (2Cys-MoPrP) labelled with tetrazine by using 10 mM and 50 mM of MEA, a reducing agent for protein disulfide bond, could be visualized by using the fluorescent image analyzer. The analysis showed that tetrazine was labelled at only both ends of the 2Cys-MoPrP. Note: (a) The fluorescent image of SDS-PAGE gel after the electrophoresis and (b) Image of SDS-PAGE gel stained with Coomassie blue overnight. Lanes 1,11 are the protein ladder, and lane 6 is empty. Lanes 2, 10 are the WT-MoPrP and Cy5-TCO. Lanes 3, 4 and 5 have Cy5-TCO and the WT-MoPrP labelled with tetrazine by using MEA at the concentration of 5mM, 10 mM and 50 mM, respectively. Lanes 7, 8, 9 have Cy5-TCO and the 2Cys-MoPrP labelled with tetrazine by using MEA at the concentration of 5mM, 10 mM and 50 mM, respectively.

In order to quantify the protein labelling with tetrazine, the mouse prion protein was diluted to the final concentration of 20  $\mu\text{M}$  and measured fragmentation spectra using mass spectrometry. The mass of the labelled mouse prion proteins showed the highest peak at 19,570 atomic mass unit (amu), consisting of the mass of mouse prion proteins and two tetrazine molecules. The result indicated that two locations of the cysteine amino acids within the proteins were labelled by two tetrazines for the attachments to the TCO DNA handles at both residues using click chemistry attachment. However, there was a peak at 18,539 amu, representing the mass of bare PrP, and also a peak at 19,129 amu, representing one tetrazine molecule and MEA, the reducing agent for the protein labelling. Thus, the highest peak of the two tetrazine labels, the suitable constructs for the single-molecule studies, lead to the higher possibility of the handle attachments at both ends of proteins rather than only one end of the proteins.

Furthermore, the structural composition of the labelled mouse prion protein that successfully attached to the DNA handle was checked by using CD Spectroscopy. The result indicated that the structure of mouse prion protein had largely alpha helical content that corresponded to the expectation, whereas the mouse prion protein labelled with tetrazine showed different CD spectrum (Requena and Wille, 2014; Riek et al., 1996).

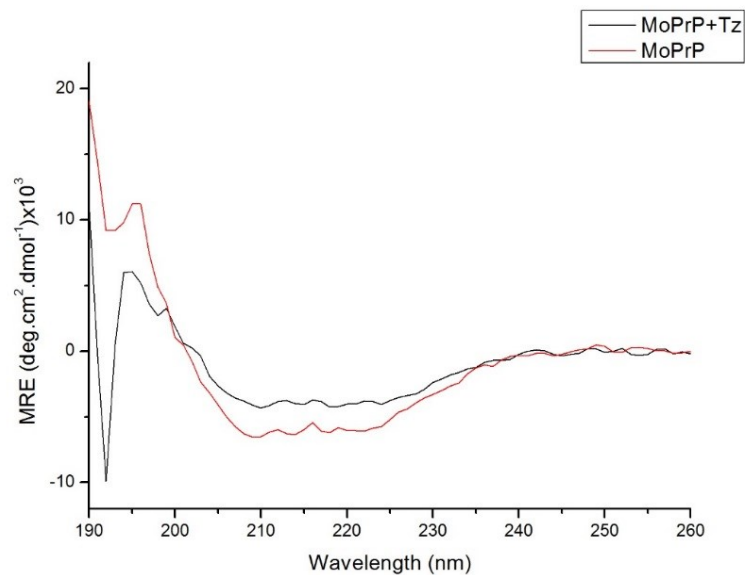


**Figure 3.11 Representative CD Spectrum of mouse prion and mouse prion protein labelled with tetrazine.** The CD spectrum of the mouse prion protein labelled with tetrazine (MoPrP+Tz) was different from the CD spectrum of the mouse prion protein before the labelling (MoPrP).

### **3.3 DNA Handles**

After the properly folded mouse prion protein was labelled with tetrazine, DNA handles were prepared in order to attach to the protein for the single-molecule force spectroscopy measurements. Functionalized DNA primers were purified by Reverse-Phase High Performance Liquid Chromatography (RP-HPLC) and the DNA templates were amplified by the polymerase chain reaction (PCR) according to the following procedures.

#### **3.3.1. Preparation of DNA primers**

The deoxyribonucleic acid oligonucleotides (DNA oligos)-Trans-Cyclooctene (TCO) primers in this experiment were prepared by following a protocol developed by Derek Dee. 1 mg of TCO-N-Hydroxysuccinimide (NHS) Ester (TCO-NHS, Product code: 1016) from the Click Chemistry Tool was dissolved in 10  $\mu$ l DMSO to a final concentration of 200 mM, and the DNA oligo-NH<sub>2</sub> from Integrated DNA Technologies was dissolved in 35  $\mu$ l of Runing Buffer (100 mM KH<sub>2</sub>PO<sub>4</sub> and 150 mM NaCl, pH 7.5) to a final concentration of 5.1 mM, respectively. Then, 5  $\mu$ l of TCO-NHS and 35  $\mu$ l oligo-NH<sub>2</sub> were combined and reacted for more than 1 hour at room temperature. After that, 2  $\mu$ l of the solution was diluted to a final concentration of 170  $\mu$ M with water for the product identification test by Reverse-Phase High Performance Liquid Chromatography (RP-HPLC) using the 1100 Series HPLC System from the Agilent Technologies.

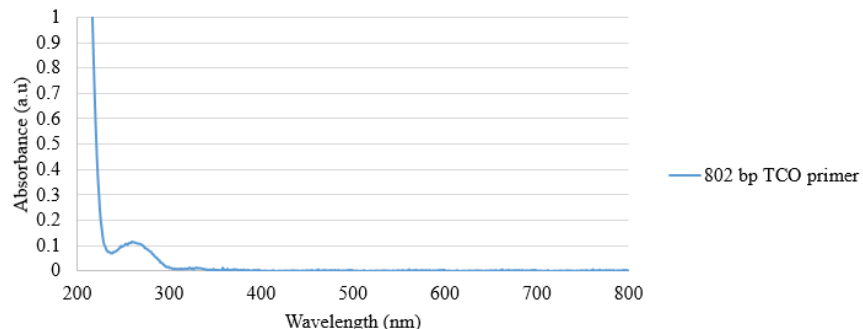


**Figure 3.12 The ultraviolet absorption of the collected 802 bp (base pairs) TCO primer.** The concentration of the DNA primer after the purification using RP-HPLC can be obtained by using the absorbance value at 260 nm for the calculation.

The rest of the solution was dispensed into two prepared tubes (19  $\mu$ l per tube) and was purified by RP-HPLC. Then, the absorbance of the collected DNA oligo - TCO primer was measured at a wavelength of 260 nm ( $A_{260}$ ) using UV-Vis. In order to check the quality of the TCO primers using click chemistry attachment, the DNA oligo - TCO primer was diluted to the final concentration of 100  $\mu$ M, mixed with DMSO to the final concentration of 5%, and run on RP-HPLC. After that, another 100  $\mu$ M of the TCO primer was combined with 250  $\mu$ M of Cy5-Tetrazine (Cy5 Tz, Product code: 1189) from the Click Chemistry Tools by mixing 500  $\mu$ M of Cy5-Tetrazine with DMSO to the final concentration of 10%. Then, both samples were run on RP-HPLC for the comparison between oligo-TCO peak and oligo-Cy5 peak.

Furthermore, the quality of the TCO primer could be checked by measuring the absorbance at a wavelength of 260 nm (the DNA primer) and 647 nm (the Cy5-Tetrazine reaction) of the collected DNA primer and the TCO DNA primer mixed with Cy5-Tetrazine.

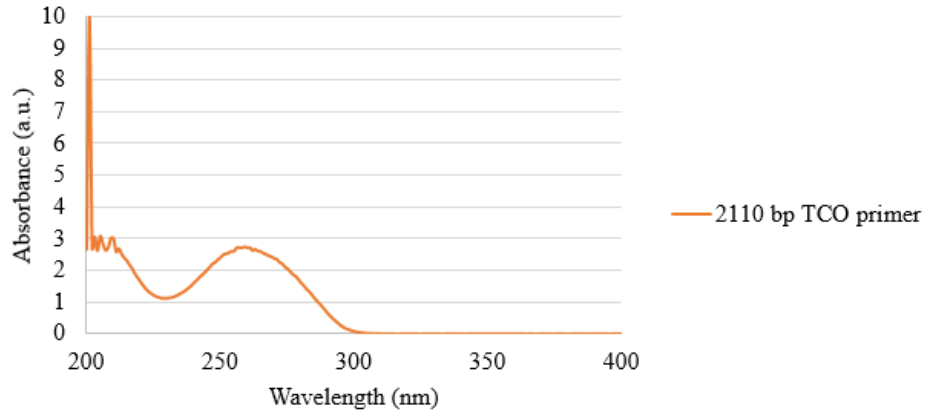


**Figure 3.13** The ultraviolet absorption of the collected 2110 bp TCO primer. The peak at 260 nm of the ultraviolet absorption curve indicated the presence of DNA primers from the reaction which was purified by using RP-HPLC

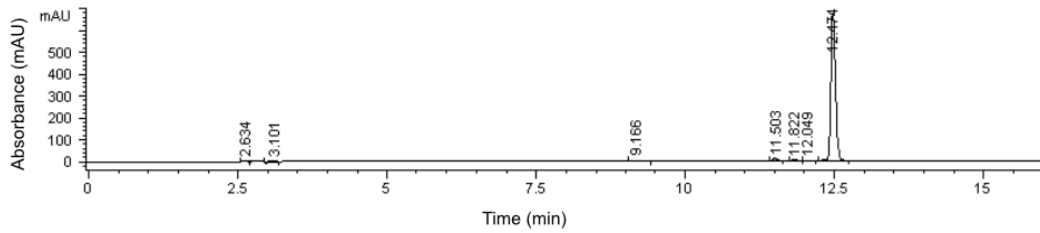


**Figure 3.14** HPLC profile of the 250  $\mu$ M of Cy5-Tetrazine for the quality control. Since there are many products as a result of the reaction for the preparation the DNA primer, Cy5-Tetrazine can be used to check the success of the TCO DNA primer preparation.

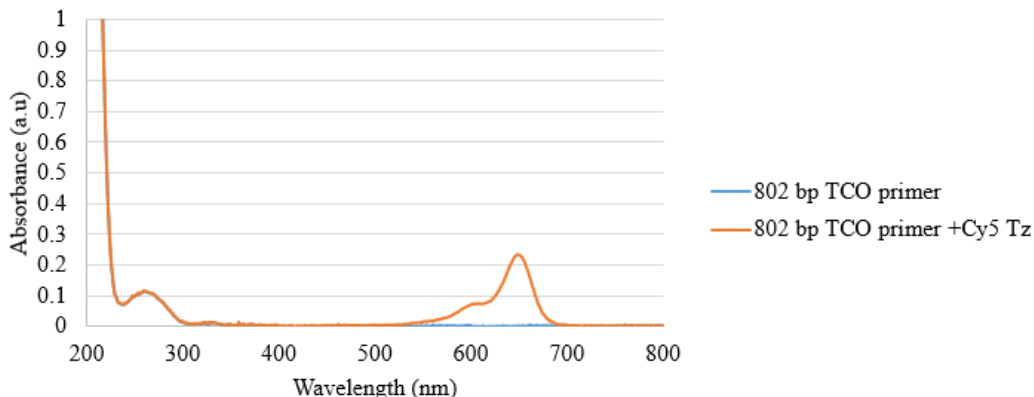


**Figure 3.15 UV absorbance spectra of the TCO primer and the TCO primer + Cy5-Tetrazine (Cy5 Tz).** The absorbance peak at 260 nm of the ultraviolet absorption curve indicated the presence of DNA primer; the concentration of the DNA primer can be obtained by using this absorbance value for the calculation. However, in-between 550-700 nm, the absorbance curve of TCO primer + Cy5-Tetrazine, showed a different shape compared to TCO primer alone, resulting from the absorption of the Cy5-Tetrazine.

### 3.3.2. Preparation of DNA handles

The DNA handles in this experiment were prepared using the polymerase chain reaction by the following protocols, adapted from previous work (Yu et al., 2012). Table 3.1 shows the amount of materials mixed, and table 3.2 shows the set-up procedure of the PCR machine. First of all, the sample was mixed and then transferred to the PCR machine. After the PCR cycle was completed, the sample was transferred to 50 ml centrifuge tube followed by the addition of 1 ml of 3 M NaOAC pH 5.2 and 30 ml of 95 % ethanol, and then it was placed overnight at 4°C. The mixture was separated by centrifugation at 14000 rpm for 20 minutes at 4°C, the pellet was rinsed with 70% ethanol and span down using the centrifugation at 14000 rpm for 20 minutes. In order to remove salts, the pellet could be rinsed and span down for at least 3 times. Next, the supernatant was

carefully discarded, the pellet was briefly air-dried for 5 minutes, dissolved in 1 ml of water and transferred to a 1.5 ml eppendorf tube. After that, the sample was run through 100K MWCO Amicon Spin Column (0.5ml) using the centrifugation at 14000 rpm for 4.5 minutes for at least 3 times, in order to remove the excess primer. Finally, the handle sample was measured on the absorbance curve at a wavelength of 260 nm ( $A_{260}$ ) using UV-Vis to find the final concentration of the handle, and diluted sample was run on 1% Agarose gel (100 minutes at 100 V) to check the quality of the DNA handle.

**Table 3.1 PCR Mixure for DNA handle**

Materials	Master Stock Concentration	Volume of Stock
Template (pMLuc 1)	35.8 ng/ $\mu$ l	10.0 $\mu$ l
Forward Primer (MW-2110bp-A-Dig-F or MW-1265bp-A-Dig-F or MW-801bp-B-TCO-F)	20.0 $\mu$ M	200.0 $\mu$ l
Reverse Primer (MW-2110bp-A-TCO-Ror MW-1265bp-A-TCO-R or MW-801bp-B-Biotinteg-R)	20.0 $\mu$ M	200.0 $\mu$ l
Deoxynucleotide (dNTP) Mix	20.0 mM	200.0 $\mu$ l
Taq DNA Polymerase	5.0 units/ $\mu$ l	50.0 $\mu$ l
10x Taq Buffer with KCl	-	1000.0 $\mu$ l
Magnesium chloride ( $MgCl_2$ )	25.0 mM	1.0 $\mu$ l
Water ( $H_2O$ )	-	7040.0 $\mu$ l
TOTAL	10,000.0 ul (10.0 ml)	

**Table 3.2 The PCR program set-up**

TCO Handle A			TCO Handle B		
Lid Temperature = 105.0 °C					
No.	Temperature	Time	No.	Temperature	Time
1	94.0 °C	0:00:01	1	94.0 °C	0:00:01
2	Pause press enter		2	Pause press enter	
3	94.0 °C	0:05:00	3	94.0 °C	0:05:00
4	94.0 °C	0:00:30	4	94.0 °C	0:00:30
5	58.2 °C	0:00:30	5	56.2 °C	0:00:30
6	72.0 °C	0:02:30	6	72.0 °C	0:01:30
7	Go to No.4-6 and repeat 35 times		7	Go to No.4-6 and repeat 26 times	
8	72.0 °C	0:05:00	8	72.0 °C	0:05:00
9	4.0 °C	Hold	9	4.0 °C	Hold
10	End		10	End	

In order to prepare the agarose gel, 80 g of agarose powder from Fisher Scientific Company was mixed with 80 ml of the ten-fold dilution of 10 x Tris-borate-ethylenediaminetetraacetic acid buffer (10xTBE buffer) in a microwaveable flask. 10xTBE buffer was prepared by mixing of 121.1 g of UltraPure™ Tris Buffer (Powder format, Product code: 15504020) from the Invitrogen™, 61.8 g of Boric acid (Powder, Product code: A74) from the Fisher Scientific Company, 7.4 g of EDTA and 1 L of water. The mixture was microwaved for 1-3 minutes until it was completely dissolved and was then poured into a gel tray. After the agarose gel cooled, the gel box was filled with 1xTBE buffer and the sample was loaded into each well of the gel. The gel was run at 100 V for 100 minutes and then was placed into a container filled with ethidium bromide (EtBr). Finally, the DNA handles were visualized using the UV light.

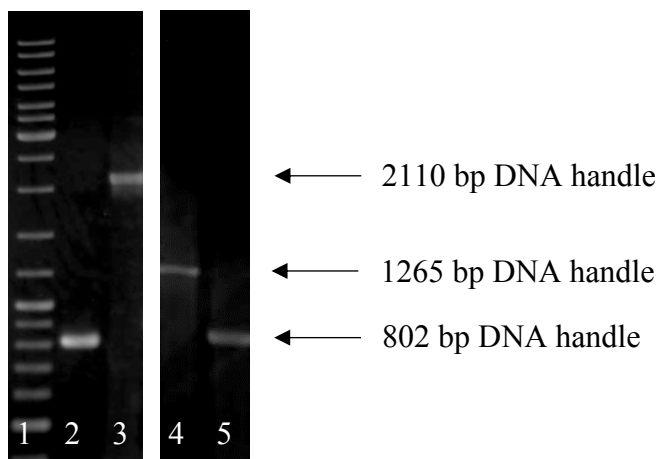


**Figure 3.16 Representative agarose gel electrophoresis of the DNA handle.**  
 Note: Lane 1 is DNA Ladder, lanes 2 and 5 are the 802 bp DNA handle, lane 3 is the 2110 bp DNA handle and lane 4 is the 1265 bp DNA handle.

### 3.3.3. Attachment of prion protein and DNA handles

The protein labelled with tetrazine can be attached to the DNA handles using the click chemistry attachment as shown in the figure 3.17. The tetrazine modified protein was mixed with TCO-DNA handles using an approximate 1:1:1 mixture of the labelled protein, TCO handle A and TCO handle B, and then it was placed overnight at 4°C. The quality of the protein-DNA handle attachment can be checked by running the diluted sample on 1% agarose gel (100 minutes at 100 V).

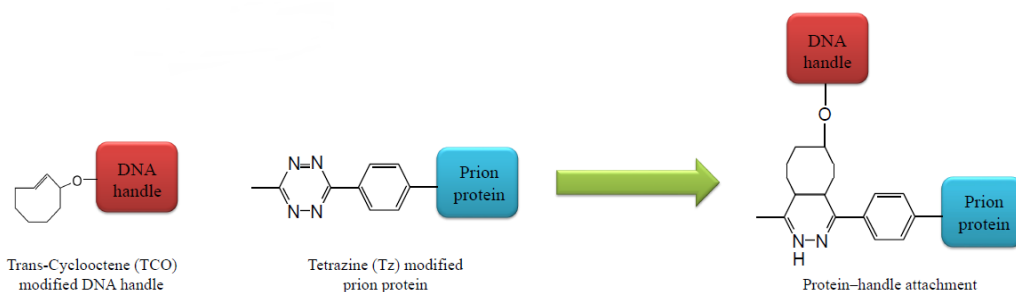


**Figure 3.17 Reaction scheme for conjugation of tetrazine-modified protein with TCO modified handle.**

However, during the first period of this experiment, the mouse prion protein labelled with tetrazine could not attach to the DNA handle successfully. In order to check the quality of the TCO DNA handle, the DNA handles were linked together following a method developed by Derek Dee. By using the click chemistry attachment, the handles were mixed with bis-tetrazine-PEG using an approximation ratio of 1:1:1. After that, the mixture was placed overnight at 4°C and then run on 1% agarose gel. The results showed the successful DNA handle – DNA handle attachment indicating that there was nothing wrong with the DNA handles or the reaction conditions as shown in figure 3.18. After the problem of the protein – handle attachment was solved by making sure that the protein was properly folded before labelling with tetrazine, the successful results of the attachment showed the combinations of protein and handle attachments compared to the handle and handle attachments as shown in figure 3.19.

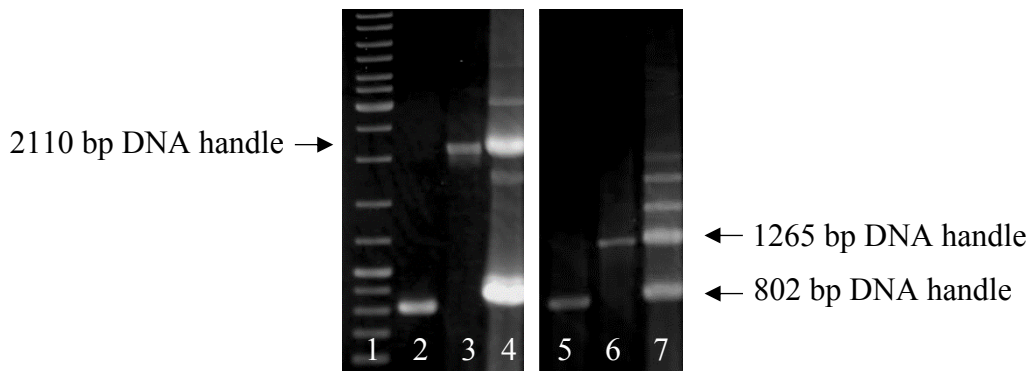


**Figure 3.18 Representative agarose gel electrophoresis of the DNA handle-DNA handle attachment.** Note: Lane 1 is DNA Ladder, lanes 2 and 5 are the 810 bp DNA handle, lane 3 is the 2110 bp DNA handle, lane 4 is the 810 bp DNA handle-2110 bp DNA handle attachment, lane 6 is the 1265 bp DNA handle and lane 7 is the 810 bp DNA handle-1265 bp DNA handle attachment.

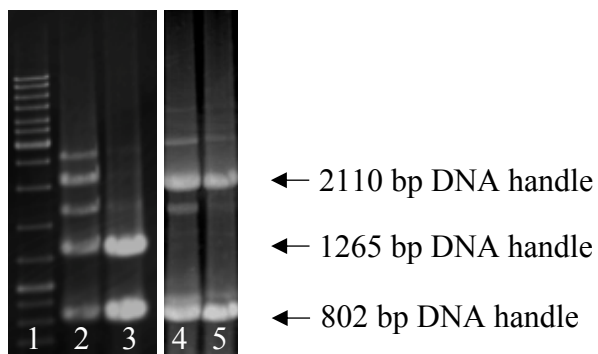


**Figure 3.19 Representative agarose gel electrophoresis of the protein-DNA handle attachment compared to the DNA handle-DNA handle attachment.** Note: Lane 1 is DNA Ladder, lane 2 is the 810 bp DNA handle-1265 bp DNA handle attachment, lane 3 is the protein-handle attachment, lane 4 is the 810 bp DNA handle-2110 bp DNA handle attachment and lane 5 is the protein-handle attachment.

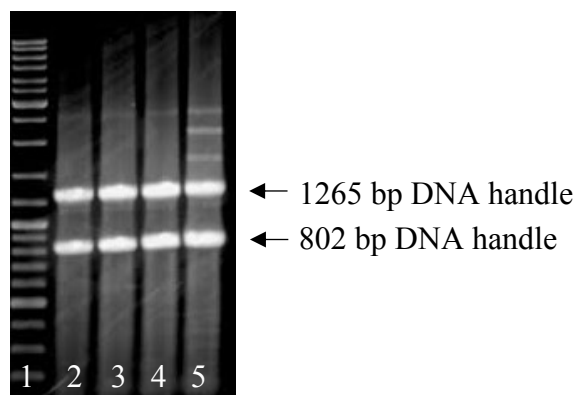


**Figure 3.20 Representative agarose gel electrophoresis of the unsuccessful protein-DNA handle attachment compared to the DNA handle-DNA handle attachment.** Note: Lane 1 is DNA Ladder, lane 2-4 are the unsuccessful protein-handle attachment and lane 5 is the protein-handle attachment.

### 3.4 Preparation for the Pulling Measurement

The shorter DNA handle was engineered to have biotin at its other end. In order to attach the handle to the bead, Avidin protein, which has strong biotin-binding ability, was used to coat the bead and make the Avidin-biotin interaction (Gitlin et al., 1987). Furthermore, the longer DNA handle was engineered to have digoxigenin at the other end. Thus, the Anti-digoxigenin (Anti-dig) was used in order to coat the other beads for the DNA handle and bead attachment. Both Avidin coated beads and Anti-dig coated beads were prepared to the final concentration of 250 pM before usage. The beads were washed separately by spinning down at 10000 rpm for 5 minutes at least 4 times and sonicated on ice for 5 minutes at 60% power. After that, 3  $\mu$ l of the diluted protein-handle attachment sample was mixed with 1  $\mu$ l of Avidin coated beads and 1  $\mu$ l of Anti-dig coated. The mixture was incubated for 1 hour at room temperature. After the incubation, 1.2  $\mu$ l of the sample was diluted into 25  $\mu$ l and loaded into a separately prepared slide. Finally, the end of the channel in the slide was blocked with grease in order to prevent the sample from drying out during the measurement.

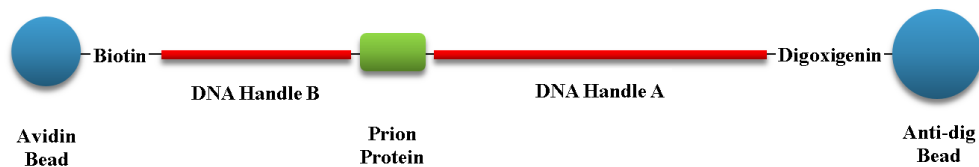


**Figure 3.21 Schematic of the sample for the pulling measurement.** The prion protein labelled with tetrazine was attached to the DNA handles. At the end of the DNA handle A and B were engineered to have biotin and Digoxigenin, respectively, resulting in the attachment to the specific beads.

## 4. Results

### 4.1. Force-Extension Curves of the Handle-Handle Attachment

According to Chapter 2, the relationship between the pulling forces and the unfolding extensions of the tethers of protein or DNA handle alone can be interpreted by analysing the Force-Extension Curves (FECs) using the wormlike chain (WLC) model. For a control experiment, the DNA handles alone were pulled by moving the optical traps at a constant speed, and the length of DNA attachment from the experiment could be compared to the length of DNA determined by the X-ray crystallography.

By using click chemistry attachment, there were two ways to attach the DNA handles together. Firstly, the TCO DNA handle was attached to another TCO DNA handle by using bis-tetrazine-PEG (Tz-PEG) as a linker. Alternatively, the TCO DNA handle was directly linked to the tetrazine (Tz) DNA handle. Thus, in this experiment, the force extension curve measurements of three different DNA handle attachments were performed under optical tweezers, namely, the 802 bp TCO and 1265 bp TCO handle attachment, the 802 bp TCO and 2110 bp TCO handle attachment, and the 802 bp Tz and 2110 bp TCO DNA handle attachment.

First, FEC measurements of the 802 bp and 1265 bp TCO handle attachment were performed as shown in figure 4.1. The force increased as a function of the DNA extension, and the analysis of the pulling curves using the WLC fitting yielded the representative contour length of handle-handle construct consisting of Tz-PEG.

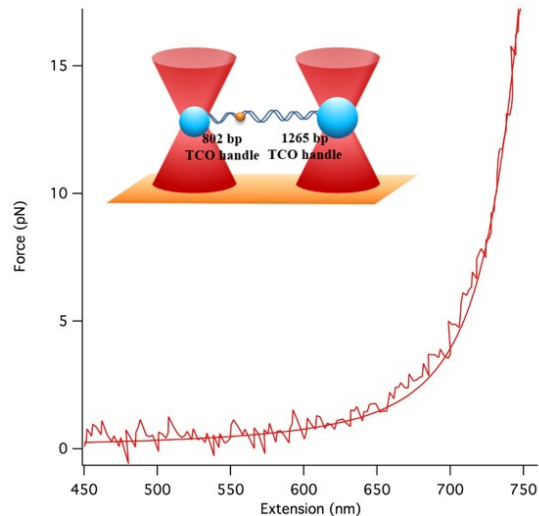


**Figure 4.1 Representative force-extension curve measurement of the 802 bp TCO and 1265 bp TCO handle attachment.** The relationship between force and extension can be interpreted by using the WLC model. Fit result:  $769.7 \pm 0.3$  nm (standard error on average from 19 FECs)

The average total contour length of this handle-handle construct consisting of Tz-PEG was  $769.7 \pm 0.3$  nm (standard error on average from 19 FECs). Note that this result differed a bit from the value calculated for the DNA handles alone (702.8 nm). This difference arises because of variations in the bead size. During data analysis, the beads are assumed to have a specific size equal to the average value; however, the actual sizes of the beads can vary by roughly  $\pm 5\%$  for each one.

Next, the contour lengths of the 802 bp and 2110 bp TCO handle attachment and the longer DNA handle attachments using Tz-PEG were measured and determined from the WLC fitting as shown in figure 4.2. The results showed that the average contour length of the DNA handle with Tz-PEG attachment was  $1217.9 \pm 0.3$  nm (average from 35 FECs), again a bit higher than expected (990.1 nm).

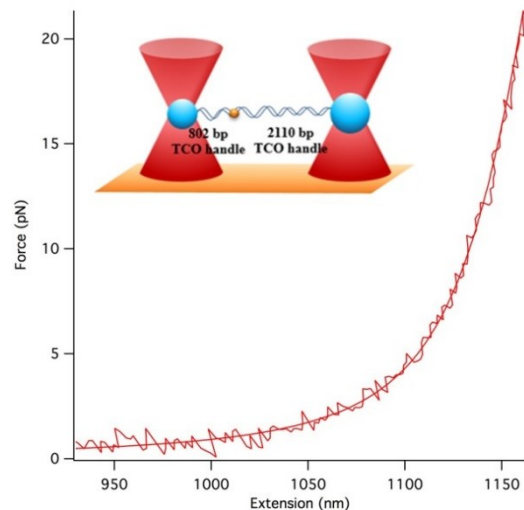


**Figure 4.2 Representative force-extension curve measurements of the 802 bp TCO and 2110 bp TCO handle attachment.** The pulling curves of the longer DNA handle attachment were interpreted resulting in the total contour length of the longer DNA handle. Fit result:  $1217.9 \pm 0.3$  nm (average from 35 FECs)

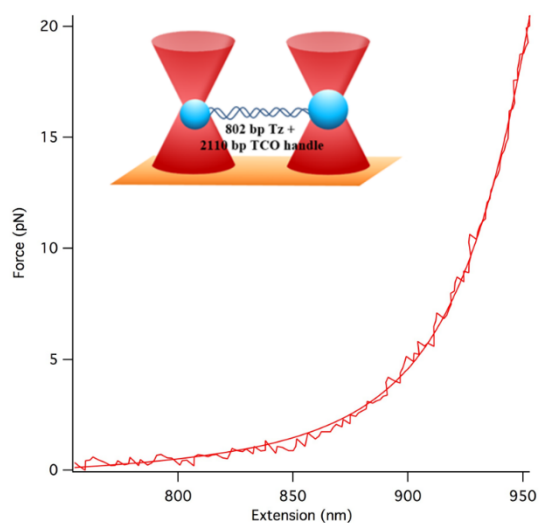


**Figure 4.3 Representative force spectroscopy measurement of the 802 bp Tz and 2110 bp TCO handle attachment.** The pulling curves of the DNA handle attachment without using Tz-PEG in between. Fit result:  $978.7 \pm 0.6$  nm (average from 11 FECs)

Finally, in order to attach both DNA handles without using Tz-PEG in between, 802 bp Tz DNA handles were made and attached directly to the 2110 bp TCO DNA handle. These constructs were measured and analyzed using the WLC model as shown in figure 4.3. The average total contour length of the DNA handles in this case was  $978.7 \pm 0.6$  nm (average from 11 FECs). The lengths obtained from WLC fitting were this time a little smaller than the expected length (990.1 nm).

## 4.2. Force-Extension Curves of the Mouse Prion Protein (MoPrP)

In order to study the contour length of the mouse prion protein for the further understanding of the behavior of MoPrP, the protein was attached to DNA handles at both ends and pulled using optical tweezers. The pulling curves of the attachment of the tetrazine labelled protein and TCO handle (using 802 bp and 2110 bp DNA handle at each end) were analyzed by the WLC model, as shown in figure 4.4. The first part of the force-extension curve represented the extension of the DNA handle attached to the folded protein, followed by a rip where the protein unfolded, whereas the last part represented stretching of both the handles and the unfolded protein.

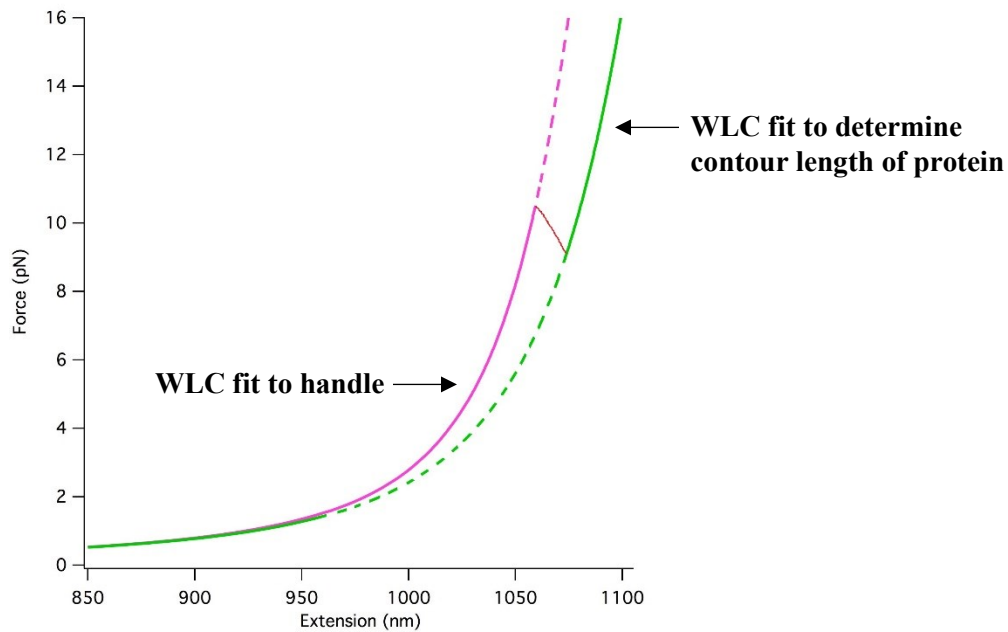


**Figure 4.4 Analysis of force spectroscopy measurement consisting of WLC fit to DNA handle (pink) and determine contour length of protein (green).** The sudden increase in the extension of the unfolding protein results in a sawtooth-shaped rip in the force-extension curve. Note: figure not drawn to scale.

The sawtooth-shaped “rip” in the force-extension curve comes from the sudden increase in the extension of the unfolding protein. Suddenly, the beads are free to move back toward the trap center, because the tether is now longer, which leads to a lower force at the same time as the extension jumps higher in the force-extension curve. The contour length change from the unfolded protein is the length of the protein backbone minus the distance between the attachment points in the folded protein, as shown in figure 4.5.

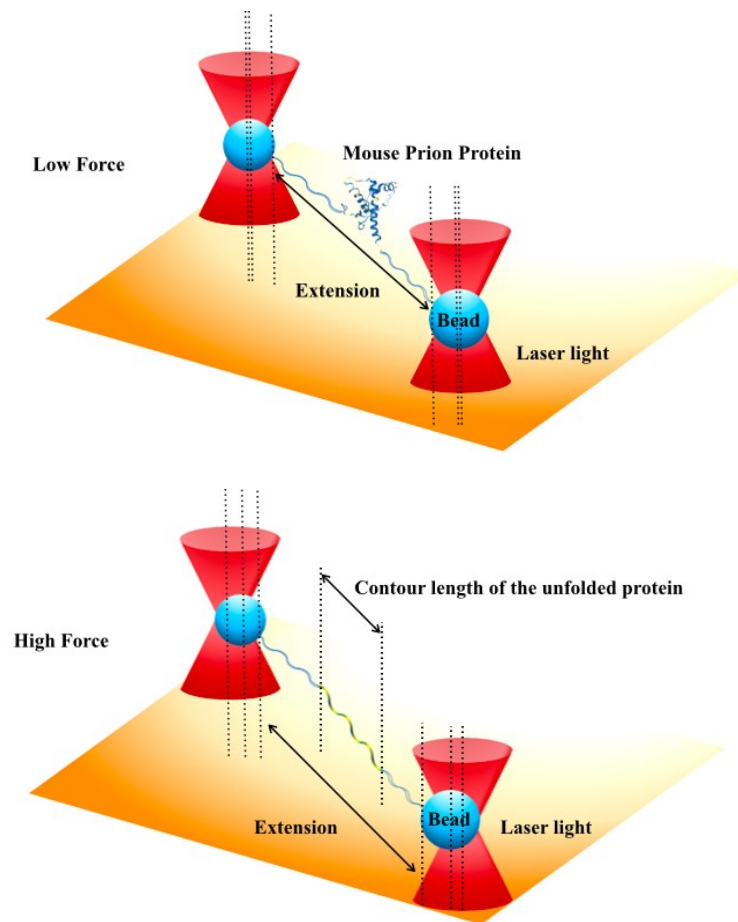


**Figure 4.5 Optical tweezers apparatus for the mouse prion protein stretching experiment.** Forces are measured from the displacement of the bead out of the trap centre, and extensions are measured from the distance of the protein and DNA handles in between both beads. Note: figure not drawn to scale.

As a result of this experiment, the average contour length of this protein-handle attachment sample from the WLC model was  $34.5 \pm 0.7$  nm (average from 6 FECs), which was close to the total length of this mouse prion protein construct from the calculation (34.3 nm).

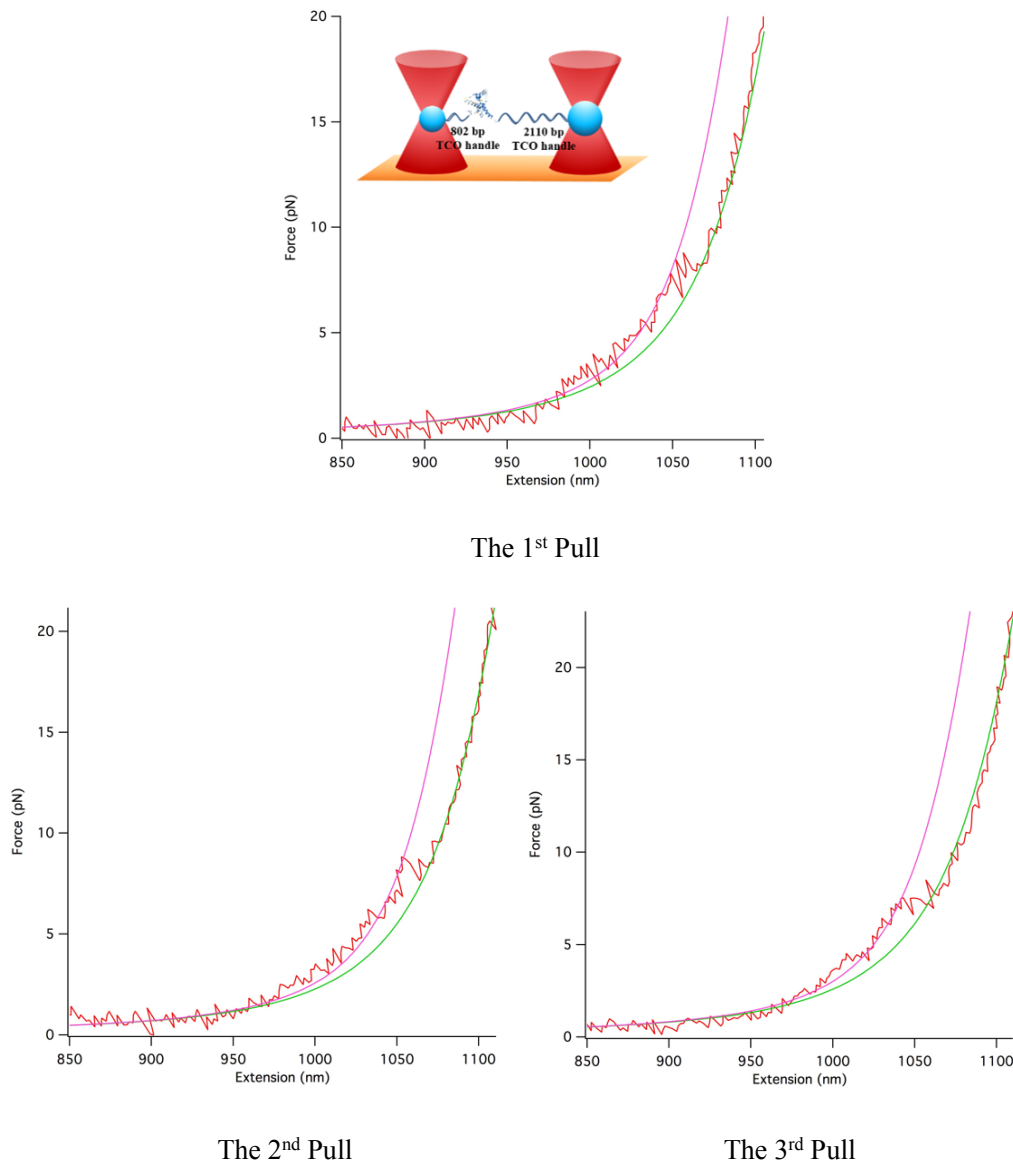


**Figure 4.6 Representative force-extension curve measurement of the mouse prion protein attached to the 802 bp TCO and 2110 bp TCO handle.** The force-extension curves of mouse prion proteins showed the folding state (pink) and unfolding state (green). At the first time, the curve represented the extension of the DNA only. After the unfolding rip, the protein-handle attachment was analyzed resulting in the contour length of the mouse prion protein.

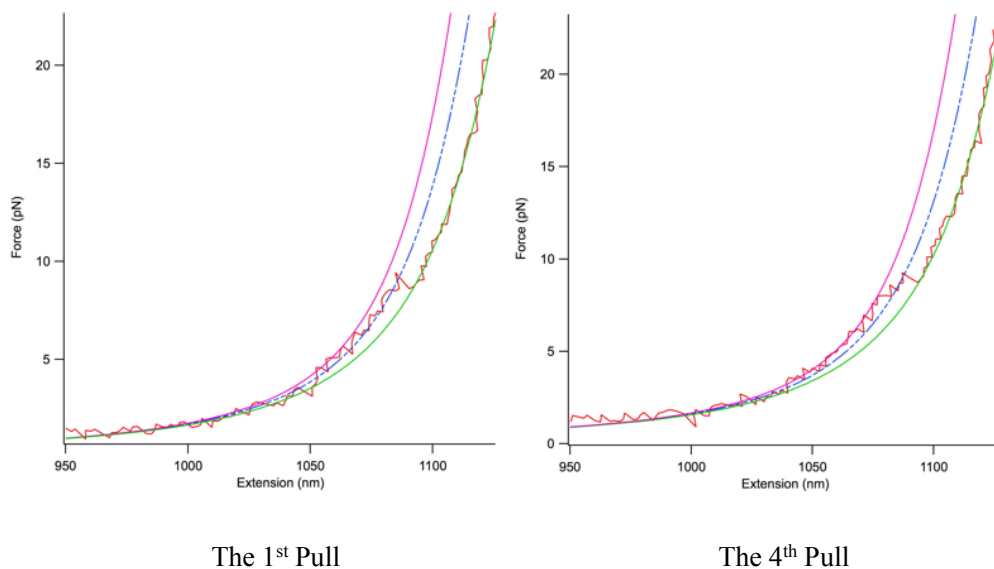


**Figure 4.7 Example of incorrectly formed tethers of the mouse prion protein attached to the 802 bp TCO and 2110 bp TCO handle.** The force-extension curves of mouse prion protein indicated three states of folding (pink), partially folded intermediate (blue) and unfolding (green).

Unfortunately, incorrectly formed tethers can occur in the experiment, in which the protein has a length that is too short, as shown in figure 4.7. The average protein contour length from this measurement was  $25.4 \pm 0.4$  nm (average from 47 FECs). There are two possible reasons why this molecule showed a shorter contour length change. First, the unfolding force might unfold only part of the protein. Thus, some part of the protein remained folded, resulting in the shorter total extension than the actual total length of the protein (34.3 nm); however, the measurement pulled up to over 20 pN of force, which should be enough to unfold PrP (Yu et al., 2012; 2015). Second, the DNA handles might not have been attached to the cysteine residues at each end of the protein. In order to attach the protein to the TCO DNA handle using click chemistry, the protein was labelled by tetrazine at cysteine (C) amino acid residue. The protein was

modified to have cysteines at each end for the labelling, but there are also two cysteine residues in the regular sequence of protein. Therefore, the shorter length may have resulted from a DNA handle attaching to an internal cysteine.

From the WLC fitting, the contour length change in the “incorrect” experiments was about 25.4 nm shorter than expected from the structure of MoPrP (34.3 nm), corresponding to approximately 24 amino acid residues. Coincidentally, there are 17 amino acid residues between the cysteine at the end of the protein construct ( $C_3$ ) and one of the cysteine residues within the mouse prion protein structure ( $C_2$ ), as shown in figure 4.8. Thus, the contour lengths from the fitting suggest that, if the protein is still folded properly, then one of the DNA handles could have been incorrectly attached to the internal cysteine  $C_2$ , whereas the other DNA handle was attached to the correct cysteine residue at the end of the protein.

Incorrectly formed tethers like this can therefore be a problem for the experiment. However, they can be detected by checking the contour length change during unfolding: FECs like the ones in figure 4.6 that have the length expected for complete unfolding of MoPrP must come from molecules with correct handle attachments.



### **4.3. Force-Extension Curves of Prion Proteins from Different Species**

Resulting from optical tweezers, the behavior of the mouse prion protein can be studied in terms of the molecular level. According to the ability to transmit prion disease, mice have a lower susceptibility to the disease than hamsters, yet a higher susceptibility than rabbits (Fernandez-Funez et al., 2011; Nyström and Hammarström, 2014). However, there are only a few different residues between hamster and mouse prion proteins. If the folding processes of both molecules were different, these residues may be one effective way of understanding the behavior of prion proteins from different species, including therapeutic drugs in the future.

The force-extension curve measurements in this work from mouse prion proteins showed not only the contour lengths of proteins, but also the unfolding forces. Since the overall thermodynamic stability of prion protein from one species should be fairly similar to the next species, the results from this work also indicated that the unfolding forces in mouse prion proteins were closely matched to hamster prion proteins as shown in figure 4.9.

Furthermore, the behavior of the hamster prion proteins showed only two states on the native pathway (folded and unfolded states), whereas the result from rabbit prion proteins indicated the presence of multiple partially folded intermediate states as shown in figure 4.9. and figure 4.10.

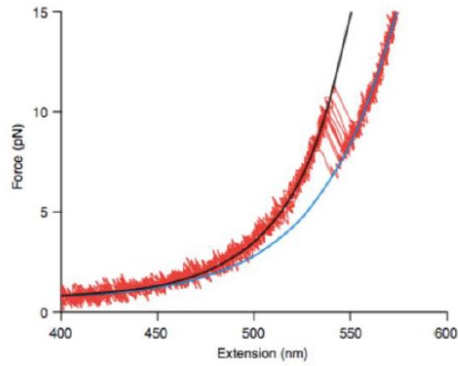


**Figure 4.9. Representative force-extension curve measurements of hamster prion protein from Hao Yu.** The behavior of the unfolding protein in details of the hamster prion protein indicated only two states of the folding and unfolding.

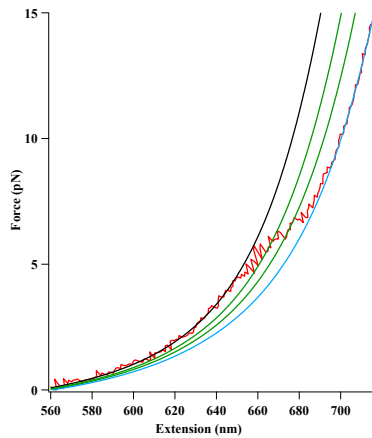


**Figure 4.10. Representative force-extension curve measurements of rabbit prion protein from Uttam Anand.** The behavior of the unfolding protein in details of the rabbit prion protein showed more complex force-extension curves compared to the native hamster prion protein, indicating the intermediate folding behavior.

As a result of the indication of the mouse extension curves according to the figure 4.6. and 4.7., mice and hamsters had closer similarities in the unfolding behavior rather than rabbits.

To illustrate the differentiations inside the structure of the prion proteins, the comparison of amino acids within these constructs are shown in figure 4.11.

There are only a few different residues between hamster and mouse, for instance, the amino residue of a hamster is leucine (L) at the location of 139, in which a mouse is isoleucine (I). However, the residues at the location of 156 and 169 of the hamster are asparagine (N), whereas the amino acids of the mouse at these locations are tyrosine (Y) and serine (S), respectively.

According to previous studies of mutation in human PrP, only one amino acid difference can cause the different form of prion protein and lead to the disease (Asante et al., 2015; Mastrianni, 2010; Yin et al., 2007). Thus, the very small dissimilarities in the prion protein sequence in the different species may help to shed more light on how sequence affects the folding. For example, the hamster and mice FECs are very similar, so the amino acid changes do not seem to change the folding significantly; however, the amino acid changes in rabbit PrP cause a much larger change in the folding. Presumably, one or more of these amino acids is the key for understanding why rabbits are quite resistant to the disease. Nevertheless, a more complete study of the differences between the folding of PrP from different species is needed in future work in order to make reliable conclusions about how sequence changes affect the folding and how these differences in folding relate to disease susceptibility.

Hamster 90	GQGGGTHNQW	NKPSKPKTNL	KHVAGAAAAG	AVVGGLGGYM	LGSAMSRPML
Mouse	GQGGGTHNQW	NKPSKPKTNL	KHVAGAAAAG	AVVGGLGGYM	LGSAMSRPMI
Rabbit	GQGGGTHNQW	GKPSKPKTNL	KHVAGAAAAG	AVVGGLGGYM	LGSAMSRPLI
				-----β1-----	
Hamster 140	HFGNDWEDRY	YRENMNRYPN	QVYYRPVDQYN	NQNNFVHDCY	NITIKQHTVT
Mouse	HFGNDWEDRY	YRENMYRYPN	QVYYRPVDQYS	NQNNFVHDCY	NITIKQHTVT
Rabbit	HFGNDYEDRY	YRENMYRYPN	QVYYRPVDQYS	NQNSFVHDCY	NITVKQHTVT
	-----α1-----		---β2---	-----α2-----	
Hamster 190	TTTKGENFTE	TDVKMMERVV	EQMCVTQYQK	ESQAYYDGRR	S
Mouse	TTTKGENFTE	TDVKMMERVV	EQMCVTQYQK	ESQAYYDGRR	S
Rabbit	TTTKGENFTE	TDVKIMERVV	EQMCITQYQQ	ESQAAYQRAA	G
	-----	-----α3-----			

**Figure 4.11. The sequence of hamster, mouse and rabbit prion proteins.** The residues highlighted in green represent important residues defined by the species barriers between hamsters and mice, whereas the red ones indicate the different amino acids of both species compared to rabbits.

## 5. Future Work

This is the first work looking at the differences between prion proteins from different species at the single-molecule level. Since the understanding of prion proteins including the effective mechanism in treating the prion diseases is not yet clearly known due to the complexity of the problem, single-molecule studies of the prion protein may result in gathering more detailed information on the misfolding without being obscured by ensemble averaging. Thanks to the advantage of the single-molecule force spectroscopy (SMFS) studies, the behavior of the prion protein can be understood in terms of the energy landscape in single-molecule level. Further studies should be done in order to clearly understand the differences between the transmission and disease susceptibility; this research can lead to a better comprehension of the protein misfolding aggregations, the disease-related mutations, and the specific treatment in the future.

First, in order to quantify the differences between mouse and hamster, the prion protein of mouse, having a lower susceptibility to the misfolding underlying prion diseases than hamster, should be studied at the same level of detail as that of hamster. Optical tweezers have been used in the studies of single molecules of hamster prion protein in the monomers (simplest aspect); they also have been used in the studies of dimers by linking two monomers together for the study of protein aggregation behavior, and the trimers (Yu et al., 2013; 2015). The results showed that the hamster prion protein in the dimer and trimer formation had more complex folding pathway than the two states folding pathway of the native structure. Furthermore, the behavior of the hamster prion protein in

previous studies was interpreted in terms of the single-molecule level leading to a better understanding of the protein misfolding aggregations including the folding kinetic, the folding pathway, the partially folded intermediates of the more complex formation of hamster prion proteins, the misfolded states and the energy landscape. Since there are a few differences in amino acid residues within the protein structures of hamster and mouse prion proteins, these residues may be an effective way to understand the differences between mouse and hamster prion protein if the folding processes of both molecules were different.

Next, in order to branch out and compare the differences between other species having different susceptibilities and resistances to the prion diseases, the studies of the relationship between the prion protein behaviors from different species compared to the effect of the different amino acid residues between each species would be one of the key areas to comprehend another understanding related to the species barriers. Furthermore, the deeper understanding of the key amino acid residues or the deeper compositions for the specie differences can be studied by using the single-point mutation prion proteins in both shorter lengths for the specific information and full length for the protein behavior in reality.

In order to understand the treatment of the prion diseases for the specific detail, the differences in the interaction between a given anti-prion compound and prion proteins from each species or specific single-point mutation constructs could be interesting. The study of the effect of a tetrapyrrole, an anti-prion compound, on the hamster prion protein in terms of single molecule has been conducted (Gupta et al., 2016). The results indicated that the unfolding force

was significantly increased when the native protein structure was bound by the compound. Furthermore, the intermolecular interaction was interfered with the ligand binding resulting in a similar behavior to the chaperones. Thus, detailed studies of the prion proteins in each species, especially in terms of the relationship between the specific amino acid residues or small compositions in protein structure and the folding behavior, can lead to a better understanding of the differences in disease transmission between species; the results from the interaction between prion proteins and a given anti-prion compound in the single-molecule level could lead to the specific therapeutic treatment in the future.

Therefore, to learn more about the prion diseases, the SMFS studies of prion protein should be conducted in 6 ways parallel to each other.

1. The SMFS studies of monomer prion protein from different species to understand the relationship between the species barriers and the folding mechanism in terms of different residues in the protein structure
2. The SMFS studies of mutation prion protein to understand the relationship between disease, mutation, aggregation, and folding pathway
3. The SMFS studies of the folding and misfolding pathway of dimer and tetramer of the prion protein in each species to understand the mechanism of the aggregation leading to approaches the treatment of the prion diseases, including the structural properties of amyloid prion protein

4. The SMFS studies of the relationship between the effects of each prion compound to the DNA handle in order to understand the mechanism of the DNA handle in the compound solution
5. The SMFS studies of the relationship between the effect of each compound including another anti-prion treatment on the protein folding pathway in different species to understand the mechanism of the interaction between the protein and the therapy
6. Integration of the SMFS studies with the computer simulation in order to enhance the understanding of the prion protein structural model and the specific treatment

Furthermore, future research on the molecular mechanisms of the prion proteins may be able to shed more light not only on the better understanding of the prion diseases, but also on the key areas to clear up other related neurodegenerative diseases, such as Alzheimer's disease and Parkinson's disease, that share similar mechanisms of protein aggregation.

## Bibliography

- Abbondanzieri, E. A. and X. Zhuang. (2009). Molecular biology: Concealed enzyme coordination. *Nature* 457: 392-393.
- Abbondanzieri, E. A., W. J. Greenleaf, et al. (2005). Direct observation of base-pair stepping by RNA polymerase. *Nature* 438: 460-465.
- Aguzzi, A. and C. J. Sigurdson. (2004). Antiprion immunotherapy: to suppress or to stimulate. *Nature Reviews Immunology* 4, 725-736.
- Aguzzi, A. and M. Heikenwalder. (2006). Pathogenesis of prion diseases: current status and future outlook. *Nature Reviews Microbiology* 4: 765-775.
- Amm, I., T. Sommer, et al. (2014). Protein quality control and elimination of protein waste: The role of the ubiquitin–proteasome system. *Biochimica et Biophysica Acta* 1843 (1): 182-196.
- Anfinsen C. B. (1973). Principles that govern the folding of protein chains. *Science*. 181(4096): 223-230.
- Anfinsen, C. B., E. Haber, et al. (1961). The kinetics of formation of native ribonuclease during oxidation of the reduced polypeptide chain. *Proceedings of the National Academy of Sciences USA* 47(9): 1309-1314.
- Asante, E.A., M. Smidak, et al. (2015). A naturally occurring variant of the human prion protein completely prevents prion disease. *Nature* 522(7557): 478-481.
- Ashkin, A., J. M. Dziedzic, et al. (1986). Observation of a single-beam gradient force optical trap for dielectric particles. *Optics Letters* 11(5): 288-290.

- Ashkin, A., J. M. Dziedzic, et al. (1987). Optical trapping and manipulation of single cells using infrared laser beams. *Nature* 330(6150): 769-771.
- Bartlett, A. I. and S. E. Radford (2009). An expanding arsenal of experimental methods yields an explosion of insights into protein folding mechanisms. *Nature Structural and Molecular Biology* 16(6): 582-588.
- Berns M. W., W. H. Wright, et al. (1989). Use of a laser-induced optical force trap to study chromosome movement on the mitotic spindle. *Proceedings of the National Academy of Sciences USA* 86(12): 4539-4543.
- Bayouth, S., M. Mehta, et al. (2001). Micromanipulation of chloroplasts using optical tweezers. *Journal of Microscopy* 203(2): 214-222.
- Blackman, M.L., M. Royzen, et al. (2008). Tetrazine ligation: fast bioconjugation based on inverse-electron-demand Diels-Alder reactivity. *Journal of the American Chemical Society* 130(41): 13518–13519.
- Bouchiat, C., M. D. Wang, et al. (1999). Estimating the persistence length of a worm-like chain molecule from force-extension measurements. *Biophysical Journal* 76: 409-43.
- Brinkers, S, H. R. C. Dietrich, et al. (2009). The persistence length of double stranded DNA determined using dark field tethered particle motion. *Journal of Chemical Physics* 130(215105): 1-9.
- Brown, D. R., K. Qin, et al. (1997). The cellular prion protein binds copper in vivo. *Nature* 390: 684-687.

- Brundin, P., R. Melki, et al. (2010). Prion-like transmission of protein aggregates in neurodegenerative diseases. *Nature Reviews Molecular Cell Biology* 11(4): 301-307.
- Bustamante, C., J. F. Marko, et al. (1994). Entropic elasticity of lambda-phage DNA. *Science* 265(5178): 1599-1600.
- Bustamante, C., S. B. Smith, et al. (2000). Single-molecule studies of DNA mechanics. *Current Opinion in Structural Biology* 10(3): 279-285.
- Bustamante, C., Y. R. Chemla, et al. (2009). High-resolution dual-trap optical tweezers with differential detection: instrument design. *Cold Spring Harbor Protocols* 4(10).
- Cassard, H., J. M. Torres, et al. (2014). Evidence for zoonotic potential of ovine scrapie prions. *Nature Communications* 5: 5821: 1-9.
- Carrion-Vazquez, M., A. F. Oberhauser, et al. (1999). Mechanical and chemical unfolding of a single protein: A comparison. *Proceedings of the National Academy of Sciences USA* 96(7): 3694-3699.
- Cecconi, C., E. A. Shank, et al. (2008). Protein-DNA chimeras for single molecule mechanical folding studies with the optical tweezers. *European Biophysics Journal* 37(6): 729-738.
- Cecconi, C., E. A. Shank, et al. (2005). Direct observation of the three-state folding of a single protein molecule. *Science* 309(5743): 2057-2060.
- Chaudhuri, T. K. and S. Paul. (2006). Protein-misfolding diseases and chaperone-based therapeutic approaches. *Federation of European Biochemical Societies Letters* 273(7): 1331-1349.

- Chen, S., A. Mangé, et al. (2003). Prion protein as trans-interacting partner for neurons is involved in neurite outgrowth and neuronal survival. *Molecular and Cellular Neuroscience* 22: 227–233.
- Chen, X. and Y. W. Wu. (2016). Selective chemical labeling of proteins. *Organic and Biomolecular Chemistry* 24: 5417-5439.
- Chiti, F. and C. M. Dobson (2006). Protein misfolding, functional amyloid, and human disease. *Annual Review of Biochemistry* 75: 333-366.
- Chothia C. (1976). The nature of the accessible and buried surfaces in proteins. *Journal of Molecular Biology* 105(1): 1-12.
- Collinge, J. (2001). Prion diseases of humans and animals: their causes and molecular basis. *Annual Review of Neuroscience* 24: 519-550.
- Collinge, J. (2016). Mammalian prions and their wider relevance in neurodegenerative diseases. *Nature* 539: 217-226.
- Danilowicz, C., D. Greenfield, et al. (2005). Dissociation of Ligand–Receptor Complexes Using Magnetic Tweezers. *Analytical Chemistry* 77(10): 3023-3028.
- Davies, G.A., A. R. Bryant, et al. (2006). Prion diseases and the gastrointestinal tract. *Canadian Journal of Gastroenterology and Hepatology* 20(1): 18-24.
- Deamer, D., M. Akeson, et al. (2016). Three decades of nanopore sequencing. *Nature Biotechnology* 34: 518-254
- Devaraj, N. R., G. M. Thurber, et al. (2012). Reactive polymer enables efficient in vivo bioorthogonal chemistry. *Proceedings of the National Academy of Sciences USA* 109: 4762–4767.

- Devaraj N. K., R. Weissleder R, et al. (2008). Tetrazine-based cycloadditions: application to pretargeted live cell imaging. *Bioconjugate Chemistry* 19(12): 2297-2299.
- Devaraj, N. K., R. Weissleder. (2011). Biomedical applications of tetrazine cycloadditions. *Accounts of Chemical Research* 44(9):816–827.
- Devaraj, N. K., R. Upadhyay, et al. (2009). Fast and sensitive pretargeted labeling of cancer cells through a tetrazine/trans-cyclooctene cycloaddition. *Angewandte Chemie International Edition in English* 48(38): 7013–7016.
- Dill, K. A. and H. S. Chan (1997). From Levinthal to pathways to funnels. *Nature Structural Biology* 4: 10-19.
- Dill, K. A., B. Ozkan, et al. (2008). The protein folding problem. *Annual Review of Biophysics* 37: 289-316.
- Dobson, C. M. (2004). Experimental investigation of protein folding and misfolding. *Methods* 34(1): 4-14.
- Dudko, O. K., J. Mathe, et al. (2010). Nanopore Force Spectroscopy Tools for Analyzing Single Biomolecular Complexes. *Method in Enzymology* 475: 565-589.
- Eisele, Y. S., C. Monteiro, et al. (2015). Targeting protein aggregation for the treatment of degenerative diseases. *Nature Reviews Drug Discovery* 14: 759–780.
- Ellis, R. J. (2006). Molecular chaperones: assisting assembly in addition to folding. *Trends in Biochemical Sciences* 31(7): 395-401.

- Evans, E., K. Ritchie, et al. (1995). Sensitive force technique to probe molecular adhesion and structural linkages at biological interfaces. *Biophysical Journal* 68: 2580-2587.
- Fändrich, M., M. A. Fletcher, et al. (2001). Amyloid fibrils from muscle myoglobin. *Nature* 410: 165-166.
- Fernandez-Funez, P., Y. Zhang, et al. (2011). Pulling rabbits to reveal the secrets of the prion protein. *Communicative and Integrative Biology* 4(3): 262-266.
- Fink, A. L. (1998). Protein aggregation: folding aggregates, inclusion bodies and amyloid. *Folding and Design* 3(1): R9- R23.
- Foster, D. (2010). High resolution optical tweezers for single molecule studies of hierarchical folding in the *pubE* riboswitch aptamer. MSc thesis, University of Alberta.
- Gitlin, G., E. A. Bayer, et al. (1987). Studies on the biotin-binding site of avidin. *Biochemical Journal* 250: 291-294.
- Goldberg, A. L. (2003). Protein degradation and protection against misfolded or damaged proteins. *Nature* 426(6968): 895-899.
- Goldmann, W., N. Hunter, et al. (1994). PrP genotype and agent effects in scrapie: change in allelic interaction with different isolates of agent in sheep, a natural host of scrapie. *Journal of General Virology* 75: 989-995.
- Gossert, A. D., S. Bonjour, et al. (2004). Prion protein NMR structures of elk and of mouse / elk hybrids. *Proceedings of the National Academy of Sciences USA* 102(3): 646-650.

- Greenfield, N. and G. D. Fasman. (1969). Computed circular dichroism spectra for the evaluation of protein conformation. *Biochemistry* 8(10): 4108-4116.
- Guo, C. L., N. C. Harris, et al. (2013). Multiscale mechanobiology: mechanics at the molecular, cellular, and tissue levels. *Cells and Bioscience* 3(25): 1-10.
- Gupta. A. N., K. Neupane, et al. (2016). Pharmacological chaperone reshapes the energy landscape for folding and aggregation of the prion protein. *Nature Communications* 7: 12058.
- Hartl. F. U., A. Bracher, et al. (2011). Molecular chaperones in protein folding and proteostasis. *Nature* 475: 324-332.
- Holzwarth G. and P. Doty. (1965). The ultraviolet circular dichroism of polypeptides. *Journal of the American Chemical Society* 87(2): 218-228.
- Hueston, W. and C. M. Bryant. (2005). Transmissible Spongiform Encephalopathies. *Journal of Food Science* 70(5): R77-R87.
- Ishijima, A., H. Kojima, et al. (1996). Multiple- and single-molecule analysis of the actomyosin motor by nanometer-piconewton manipulation with a microneedle: unitary steps and forces. *Biophysical Journal* 70(1): 383-400.
- Jahn, T. R. and S. E. Radford (2005). The Yin and Yang of protein folding. *Federation of European Biochemical Societies Journal* 272: 5962-5970.
- Janshoff, A., M. Neitzert, et al. (2000). Force Spectroscopy of Molecular Systems—Single Molecule Spectroscopy of Polymers and Biomolecules. *Angewandte Chemie International Edition* 39: 3212-3237.

- Kamsma, D., R. Creyghton, et al. (2016). Tuning the Music: Acoustic Force Spectroscopy (AFS) 2.0. *Methods* 105: 26-33.
- Kellermayer, M. S., S. B. Smith, et al. (1997). Folding-Unfolding Transitions in Single Titin Molecules Characterized with Laser Tweezers. *Sciences* 276(5315): 1112-1116.
- Kelly, S. M. and N. C. Price. (2000). The use of circular dichroism in the investigation of protein structure and function. *Current Protein and Peptide Science* 1(4): 349-384.
- Kishino, A. and T. Yanagida. (1988). Force measurements by micromanipulation of a single actin filament by glass needles. *Nature* 334(6177): 74-76.
- Knowles, T. P. J., M. Vendruscolo, et al (2014). The amyloid state and its association with protein misfolding diseases. *Nature Reviews Molecular Cell Biology* 15: 384–396.
- Kurt, T. D. and C. J. Sigurdson. (2016). Cross-species transmission of CWD prions. *Prion* 10(1): 83-91.
- Lang, K., L. Davis, L., et al. (2012). Genetic Encoding of bicyclononynes and transcyclooctenes for site-specific protein labeling in vitro and in live mammalian cells via rapid fluorogenic Diels-Alder reactions. *Journal of the American Chemical Society* 134: 10317–10320.
- Levinthal, C. (1969). How to fold graciously. *Mössbauer Spectroscopy in Biological Systems Proceedings* 67(41): 22-24
- Liphardt, J., B. Onoa, et al. (2001). Reversible unfolding of single RNA molecules using mechanical force. *Science* 292: 733-737.

- Makaraviciute, A., C. D. Jackson, et al. (2016). Considerations in producing preferentially reduced half-antibody fragments. *Journal of Immunological Methods* 429: 50-56.
- Marko, J. and E. D. Siggia (1995). Stretching DNA. *Macromolecules* 28: 8759-8770.
- Martins, V. R., A. F. Mercadante, et al. (2001). Insights into the physiological function of cellular prion protein. *Brazilian Journal of Medical and Biological Research* 34(5): 585-595.
- Mastrianni, J. A. (2010). The genetics of prion diseases. *Genetics in Medicine*. 12(4): 187-195.
- Meiners, J. C. and S. R. Quake. (1999). Direct measurement of hydrodynamic cross correlations between two particles in an external potential. *Physical Review Letters* 82(10): 2211-2214.
- Micsonai, A., F. Wien, et al. (2015). Accurate secondary structure prediction and fold recognition for circular dichroism spectroscopy. *Proceedings of the National Academy of Sciences USA* 112(24): E3095-E3103.
- Moffitt, J. R., Y. R. Chemla, et al. (2006). Differential detection of dual traps improves the spatial resolution of optical tweezers. *Proceedings of the National Academy of Sciences USA* 103(24): 9006-9011.
- Morel, E., S. Fouquet, et al. (2008). The cellular prion protein PrP<sup>c</sup> is involved in the proliferation of epithelial cells and in the distribution of junction-associated proteins. *Public Library of Science One* 3(8): e3000.

- Moy, V. T., E. L. Florin, et al. (1994). Intermolecular forces and energies between ligands and receptors. *Science* 266(5183): 257-259.
- Neuman, K. C. and A. Nagy. (2008). Single-molecule force spectroscopy: optical tweezers, magnetic tweezers and atomic force microscopy. *Nature Methods* 5(6): 491-505.
- Neuman, K. C. and S. M. Block. (2004). Optical trapping. *Review of Scientific Instruments* 75(9): 2787-2809.
- Norregaard, K., R. Metzler, et al. (2017). Manipulation and Motion of Organelles and Single Molecules in Living Cells. *Chemical Reviews* 117(5): 4342-4375.
- Nyström S. and P. Hammarström. (2014). Generic amyloidogenicity of mammalian prion proteins from species susceptible and resistant to prions. *Scientific Reports* 5:10101: 1-12
- Perkins, T. T., S. R. Quake, et al. (1994). Relaxation of a single DNA molecule observed by optical microscopy. *Science* 264(5160): 822-826.
- Petrosyan, R., C. A. Bippes, et al. (2015). Single-Molecule Force Spectroscopy of Membrane Proteins from Membranes Freely Spanning Across Nanoscopic Pores. *Nano Letters* 15(5): 3624-3633.
- Plaxco, K. W. and C. M. Dobson (1996). Time-resolved biophysical methods in the study of protein folding. *Current Opinion in Structural Biology* 6(5): 630-636.

- Plummer, P. J. (1946). Scrapie – a disease of sheep: a review of the literature. *Canadian Journal of Comparative Medicine and Veterinary Science* 10(2): 49-54.
- Pool, R. (1988). Trapping with optical tweezers. *Science* 241(4869): 1042.
- Prusiner, S. B. (1982). Novel proteinaceous infectious particles cause scrapie. *Science* 216(4542): 136-144.
- Prusiner, S.B., M. R. Scott, et al. (1998). Prion protein biology. *Cell* 93(3): 337-348
- Qing, L.L., H. Zhao, et al. (2014). Progress on low susceptibility mechanisms of transmissible spongiform encephalopathies. *Zoological Research* 35(5): 436-445.
- Ramachandran, G. N., C. Ramakrishnan, et al. (1963). Stereochemistry of polypeptide chain configurations. *Journal of Molecular Biology* 7: 95-99.
- Ramakrishnan, C. (2001). Ramachandran and his map. *Resonance* 6(10): 48-56.
- Raven, P. H. and G. B. Johnson (2001). *Biology*. 6th Ed. Boston: McGraw-Hill.
- Requena, J. R. and H. Wille. (2014). The structure of the infectious prion protein: experimental data and molecular models. *Prion* 8(1): 60-66.
- Riek, R., S. Hornrmann, et al. (1996). NMR structure of the mouse prion protein domain PrP(121-231). *Nature* 382(6587): 180-182.
- Ritchie, D. B. and M. T. Woodside. (2015). Probing the structural dynamics of proteins and nucleic acids with optical tweezers. *Current Opinion in Structural Biology* 34: 43-51.

- Ross C. A. and M.A. Poirier (2004). Protein aggregation and neurodegenerative disease. *Nature Medicine* 10: S10-S17.
- Rossin, R., S. M. van den Bosch, et al. (2013) Highly reactive trans-cyclooctene tags with improved stability for Diels-Alder chemistry in living systems. *Bioconjugate Chemistry* 24, 1210–1217.
- Sacchettini, J. C. and J. W. Kelly (2002). Therapeutic strategies for human amyloid diseases. *Nature Reviews Drug Discovery* 1(4): 267-275.
- Schnabel, J. (2011). Amyloid: Little protein, big clues. *Nature* 475: S12-S14.
- Selvaraj, R. and J. M. Fox. (2013). trans-Cyclooctene-a stable, voracious dienophile for bioorthogonal labeling. *Current Opinion in Chemical Biology* 17: 753–760.
- Shingyoji, C., H. Higuchi, et al. (1998). Dynein arms are oscillating force generators. *Nature* 393: 711-714.
- Singh, A., M. L. Mohan, et al. (2009). Prion protein modulates cellular iron uptake: a novel function with implications for prion disease pathogenesis. *Public Library of Science One*, 4(2): e4468.
- Sitters, G., D. Kamsma, et al. (2015). Acoustic force spectroscopy. *Nature Methods* 12: 47-50.
- Stathopoulos, P. B., G. A. Scholz, et al. (2004). Sonication of proteins causes formation of aggregates that resemble amyloid. *Protein Science* 13(11): 3017-3027.

- Stirnemann, G., D. Giganti, et al. (2013). Elasticity, structure, and relaxation of extended proteins under force. *Proceedings of the National Academy of Sciences USA* 110(10): 3847-3852.
- Svoboda, K., C. F. Schmidt, et al. (1993). Direct observation of kinesin stepping by optical trapping interferometry. *Nature* 365(6448): 721-727.
- Soto, C. (2001). Protein misfolding and disease; protein refolding and therapy. *Federation of European Biochemical Societies Letters* 498(2-3): 204-207.
- Wang, M.D., H. Yin, et al. (1997). Stretching DNA with optical tweezers. *Biophysical Journal* 72(3): 1335-1346.
- Watanabe, T., Y. Yasutaka, et al. (2011). Involvement of the cellular prion protein in the migration of brain microvascular endothelial cells. *Neuroscience Letters* 496(2): 121-124.
- Westergaard, L., H. M. Christensen, et al. (2007). The cellular prion protein (PrP<sup>c</sup>): its physiological function and role in disease. *Biochim Biophys Acta*. 1772(6): 629-644.
- Winklhofer, K. F., J. Tatzelt, et al. (2008). The two faces of protein misfolding: gain- and loss-of-function in neurodegenerative diseases. *European Molecular Biology Organization Journal* 27(2): 336-349.
- Yin, S., N. Pham, et al. (2007). Human prion protein with pathogenic mutations share common conformational changes resulting in enhanced binding to glycosaminoglycan. *Proceedings of the National Academy of Sciences USA* 104(18): 7546-7551.

Yu, H. (2013). Single-molecule studies of prion protein folding and misfolding.

PhD thesis, University of Alberta.

Yu, H., D. R. Dee, et al. (2015). Protein misfolding occurs by slow diffusion across multiple barriers in a rough energy landscape. *Proceedings of the National Academy of Sciences USA* 112: 8308-8313.

Yu, H., D. R. Dee, et al. (2013). Single-molecule approaches to prion protein misfolding. *Prion* 7(2): 140-146

Yu, H., X. Liu, et al. (2012). Direct observation of multiple misfolding pathways in a single prion protein molecule. *Proceedings of the National Academy of Sciences USA* 109(14): 5283-5288.